



Two Functionally Redundant FK506-Binding Proteins Regulate Multidrug Resistance Gene Expression and Govern Azole Antifungal Resistance

Romila Moirangthem,^{a*} Kundan Kumar,^{a,b}  Rupinder Kaur^a

^aLaboratory of Fungal Pathogenesis, Centre for DNA Fingerprinting and Diagnostics, Hyderabad, India

^bGraduate Studies, Manipal Academy of Higher Education, Manipal, Karnataka, India

Romila Moirangthem and Kundan Kumar contributed equally to the work. Author order was determined based on initiation of the research idea.

ABSTRACT Increasing resistance to antifungal therapy is an impediment to the effective treatment of fungal infections. *Candida glabrata* is an opportunistic human fungal pathogen that is inherently less susceptible to cost-effective azole antifungals. Gain-of-function mutations in the Zn-finger pleiotropic drug resistance transcriptional activator-encoding gene *CgPDR1* are the most prevalent causes of azole resistance in clinical settings. *CgPDR1* is also transcriptionally activated upon azole exposure; however, factors governing *CgPDR1* gene expression are not yet fully understood. Here, we have uncovered a novel role for two FK506-binding proteins, CgFpr3 and CgFpr4, in the regulation of the *CgPDR1* regulon. We show that CgFpr3 and CgFpr4 possess a peptidyl-prolyl isomerase domain and act redundantly to control *CgPDR1* expression, as a *Cgfpr3Δ4Δ* mutant displayed elevated expression of the *CgPDR1* gene along with overexpression of its target genes, *CgCDR1*, *CgCDR2*, and *CgSNQ2*, which code for ATP-binding cassette multidrug transporters. Furthermore, CgFpr3 and CgFpr4 are required for the maintenance of histone H3 and H4 protein levels, and fluconazole exposure leads to elevated H3 and H4 protein levels. Consistent with the role of histone proteins in azole resistance, disruption of genes coding for the histone demethylase CgRph1 and the histone H3K36-specific methyltransferase CgSet2 leads to increased and decreased susceptibility to fluconazole, respectively, with the *Cgrph1Δ* mutant displaying significantly lower basal expression levels of the *CgPDR1* and *CgCDR1* genes. These data underscore a hitherto unknown role of histone methylation in modulating the most common azole antifungal resistance mechanism. Altogether, our findings establish a link between CgFpr-mediated histone homeostasis and *CgPDR1* gene expression and implicate CgFpr in the virulence of *C. glabrata*.

KEYWORDS human fungal pathogens, histone modifications, histone chaperones, histone H3 lysine 36 methylation, FK506-binding protein, antifungal drug resistance, multidrug efflux pump expression, H3K36me3

Successful treatment of fungal bloodstream infections (BSIs) is often restricted by the availability of a limited number of antifungal drugs and emerging resistance to existing antifungals (1–3). Polyenes, azoles, and echinocandins represent three major classes of antifungal drugs that are currently being used worldwide to treat fungal BSIs (4). Azoles block ergosterol biosynthesis by inhibiting the lanosterol 14- α -demethylase enzyme encoded by the *ERG11* gene, while echinocandins impede the synthesis of 1,3- β -D-glucan in the fungal cell wall by targeting the β -glucan synthase catalytic subunit encoded by the *FKS* genes (4). The polyene antifungals bind to ergosterol in the fungal cell membrane and cause disruption of cell membrane integrity and/or

Citation Moirangthem R, Kumar K, Kaur R. 2021. Two functionally redundant FK506-binding proteins regulate multidrug resistance gene expression and govern azole antifungal resistance. *Antimicrob Agents Chemother* 65: e02415-20. <https://doi.org/10.1128/AAC.02415-20>.

Copyright © 2021 American Society for Microbiology. All Rights Reserved.

Address correspondence to Rupinder Kaur, rkaur@cdfd.org.in.

* Present address: Romila Moirangthem, Department of Immunology, The Ruth and Bruce Rappaport Faculty of Medicine, Technion-Israel Institute of Technology, Haifa, Israel.

Received 16 November 2020

Returned for modification 1 January 2021

Accepted 6 March 2021

Accepted manuscript posted online 15 March 2021

Published 18 May 2021

ergosterol extraction from the cell membrane (4, 5). Resistance to azoles and echinocandin antifungal drugs is increasingly being reported across the world (1, 2, 6).

Candida species contribute substantially to fungal BSIs, with *Candida albicans* as the leading etiological agent (6–8). *Candida glabrata* is the second to fourth leading cause of candidemia around the world, whose prevalence has increased over the last 2 decades (6, 9–11). Many factors, including prior fluconazole exposure, older age, and geographical region, have been associated with the increased prevalence of *C. glabrata* (6, 9, 11). *C. glabrata* is intrinsically less susceptible to azole antifungals, and about 10% of *C. glabrata* isolates have been reported to be associated with fluconazole resistance in clinical settings (1, 6).

Azole resistance in clinical isolates of *C. glabrata* majorly arises from single-amino-acid substitution gain-of-function mutations in the *CgPDR1* gene (12–14), which codes for a Zn₂Cys₆ binuclear zinc cluster domain-containing transcription factor (15–17). A variety of nonsynonymous mutations in *CgPDR1* have been reported, which are associated with both azole resistance and increased virulence (12–14). CgPdr1 activates the expression of its target genes, including *CgCDR1* and *CgCDR2*, by binding to pleiotropic drug response elements (PDREs) present in target gene promoters (16–18). *CgCDR1* and *CgCDR2* encode multidrug efflux pumps belonging to the ATP-binding cassette (ABC) transporter family (13, 19, 20). *CgSNQ2* and *EPA1*, coding for an ABC transporter and an epithelial cell adhesin, are also target genes of CgPdr1 (18, 21, 22). Multidrug transporters mediate the efflux of azole drugs, thereby reducing the intracellular azole concentration and leading to drug resistance (13).

Echinocandin resistance in clinical isolates of *C. glabrata* has primarily been due to mutations in the *CgFKS1* and *CgFKS2* genes and is rising (1, 6, 23). Furthermore, up to 8% of azole-resistant isolates were found to display coresistance to echinocandins during the 2006–2016 SENTRY antifungal surveillance program (6). Recently, a new mechanism imparting multidrug resistance (MDR) in *C. glabrata* clinical isolates has been ascribed to mutations in the DNA mismatch repair gene *CgMSH2* (24); however, *CgMSH2* mutations were not always found to be associated with antifungal multidrug resistance (25–27).

Chromatin-dependent processes are increasingly being investigated for their role in fungal pathogenesis and antifungal drug resistance (28, 29). Acetylation and deacetylation of lysines in proteins, including histones, have been shown to be important for antifungal resistance (28, 30). Consistently, CgHst1 deacetylase in *C. glabrata* has been shown to negatively regulate *CgPDR1* expression, with *CgHST1* gene loss rendering cells azole resistant (31). Furthermore, HDAC (histone deacetylase) inhibitors have been reported to exhibit synergistic effects with azoles in the treatment of fungal infections (32).

In the current study, we have uncovered a novel role for two FK506-binding proteins (FKBPs), CgFpr3 and CgFpr4, which possess a peptidyl-prolyl *cis-trans* isomerase (PPIase) domain, in the regulation of histone H3 and H4 protein levels and azole antifungal resistance. Furthermore, while the *Cgfpr3Δ4Δ* mutant displayed increased basal expression of the *CgPDR1* and *CgCDR1* genes and consequent resistance to fluconazole, the loss of the histone demethylase CgRph1 resulted in increased susceptibility to fluconazole and diminished basal expression of the *CgPDR1* and *CgCDR1* genes. We also demonstrate for the first time that CgSet2 is a histone H3 lysine 36-specific methyltransferase, which negatively regulates azole resistance. Altogether, our findings unravel a whole new epigenetic layer of regulation of *CgPDR1* and *CgCDR1* gene expression that may be governed by the levels and posttranslational modifications (PTMs) of histones H3 and H4 in fungal cells.

RESULTS

CgFpr3 and CgFpr4 proteins contain a peptidyl-prolyl *cis-trans* isomerase domain at their C termini. We have previously shown that the ability to remodel its chromatin contributes to the intracellular proliferation of *C. glabrata*, and mutants disrupted for genes involved in chromatin organization displayed decreased survival in human THP-1 macrophages (33). Of 7 chromatin organization-defective mutants identified in a screen for diminished survival/replication in macrophages, one carried a Tn7

insertion in the *CgFPR4* (*CAGL0M00638g*) gene. The *CgFPR4* gene is uncharacterized in *C. glabrata*; however, its ortholog in *Saccharomyces cerevisiae* codes for a nuclear FK506-binding protein, which possesses peptidyl-prolyl *cis-trans* isomerase (PPIase) activity (34, 35). Fpr4 in *S. cerevisiae* modulates lysine methylation of histones H3 and H4 by catalyzing the isomerization of proline residues in H3 and H4, acts as an acidic histone chaperone, and is implicated in histone homeostasis (36, 37). Since a reduced histone H4 gene dosage has recently been linked with elevated resistance to DNA damage (38), we sought to examine the role of the *CgFPR4* gene in stress resistance and virulence in *C. glabrata*. *In silico* analysis identified the FKBP_C peptidyl-prolyl *cis-trans* isomerase and the nucleoplasmin-like domain (characteristic structural domain of the nucleoplasmin core domain superfamily proteins that bind to core histones and are pivotal to the assembly of nucleosomal arrays [39]) in the CgFpr4 protein (see Fig. S1A in the supplemental material). Since Fpr3 and Fpr4 constitute a paralog pair in *S. cerevisiae* and regulate the proteolysis of the centromeric histone H3 variant Cse4 (40), we next identified the ortholog of *S. cerevisiae* FPR3 in *C. glabrata* and found it to be the *CAGL0L11484g* open reading frame (ORF). The *CgFPR3* and *CgFPR4* gene loci are syntenic to the corresponding *S. cerevisiae* loci (Fig. S1B), and the CgFpr3 and CgFpr4 proteins showed 84% and 80% similarities to *S. cerevisiae* Fpr3 and Fpr4, respectively (Fig. S1C). Furthermore, similar to CgFpr4, CgFpr3 also contained the nucleoplasmin-like domain and the prolyl *cis-trans* isomerase domain at the N and C termini, respectively, with both proteins carrying a nuclear localization sequence in the midregion (Fig. S1A). This *in silico* analysis suggested that similar to their *S. cerevisiae* counterparts (36, 40, 41), CgFpr3 and CgFpr4 may have proline isomerase activity and may act as histone chaperones in *C. glabrata*.

CgFpr3 and CgFpr4 are required for maintenance of histone H3 and H4 protein levels. To study the role of CgFpr3 and CgFpr4 in histone homeostasis in *C. glabrata*, we created single-deletion strains lacking either the *CgFPR3* or *CgFPR4* gene as well as a double-deletion strain lacking both the *CgFPR3* and *CgFPR4* genes. Phenotypic characterization of the generated mutants revealed that *CgFPR3* and *CgFPR4* gene loss had no effect on the growth of *C. glabrata* under thermal (42°C), DNA damage (methyl methanesulfonate [alkylates DNA]), oxidative (hydrogen peroxide and menadione [produce reactive oxygen species]), cell wall (Congo red [inhibits the formation of two key components of the fungal cell wall, chitin and β -glucan]), and cell membrane (sodium dodecyl sulfate [SDS] [perturbs the plasma membrane]) stress conditions (Fig. 1A). Notably, the *Cgfp3 Δ 4 Δ* mutant exhibited a mild growth defect in rich yeast extract-peptone-dextrose (YPD) medium, with a doubling time of 79 min, compared to 67 min for the wild-type (wt) strain (Fig. 1B).

Next, we checked the levels of histones H3 and H4 in *Cgfp3 Δ* , *Cgfp4 Δ* , and *Cgfp3 Δ 4 Δ* mutants and found 2-fold-higher H3 and H4 levels in the *Cgfp3 Δ 4 Δ* mutant (Fig. 1C). Contrarily, H3 and H4 levels in single mutants were similar to those in the wt strain (Fig. 1C). These data suggest that CgFpr3 and CgFpr4 act redundantly to maintain the levels of two core histones, H3 and H4, in *C. glabrata*. Furthermore, to examine if CgFpr3 and CgFpr4 modulate the transcription of H3 and H4 genes, we performed quantitative real-time reverse transcriptase PCR (qPCR) to determine histone H3 (*CgHHT*) and H4 (*CgHHF*) transcript levels in log-phase cells. We found that the expression levels of both genes were similar in the *Cgfp3 Δ 4 Δ* and wt strains (Fig. 1D). These data suggest that CgFpr3 and CgFpr4 regulate histone H3 and H4 expression posttranscriptionally.

CgFPR3 and CgFPR4 genes are required for survival of *C. glabrata* in mice. Reduced histone H4 levels have recently been associated with increased biofilm formation and diminished survival of *C. glabrata* in kidneys of mice (38). Since the *Cgfp3 Δ 4 Δ* mutant contained higher levels of histones H3 and H4 (Fig. 1C), we decided to determine the role of CgFpr3 and CgFpr4 in pathogenesis. For this, we studied two virulence-associated traits, *viz.*, biofilm formation and survival, in the murine model of disseminated candidiasis. For the biofilm formation assay, we grew wt and *Cgfp3 Δ* , *Cgfp4 Δ* , and *Cgfp3 Δ 4 Δ* mutant cells in RPMI 1640 medium under static conditions

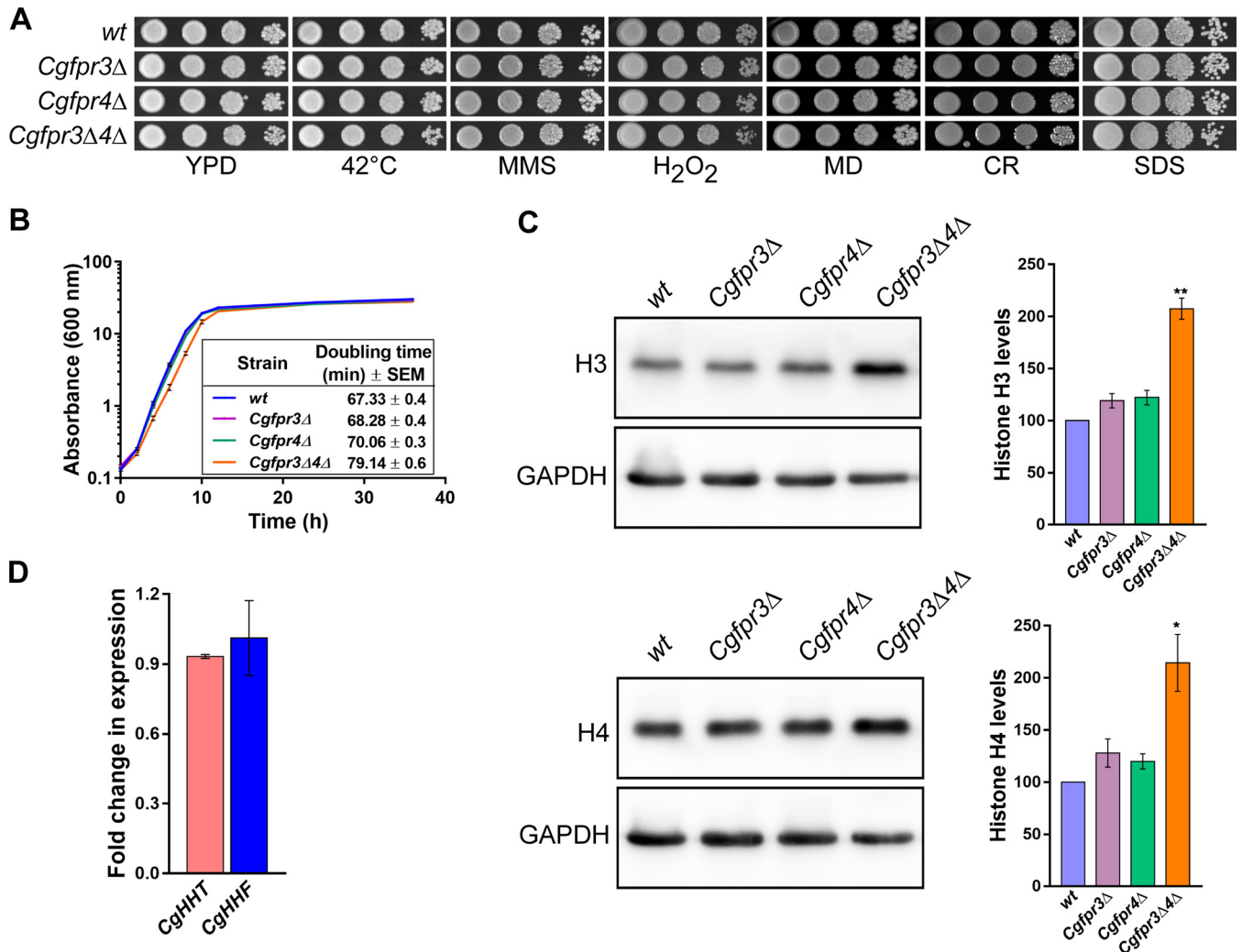


FIG 1 The *Cgfp3Δ4Δ* mutant contains elevated levels of histone H3 and H4 proteins. (A) Serial dilution spot analysis to assess the growth of the *Cgfp3Δ*, *Cgfp4Δ*, and *Cgfp3Δ4Δ* mutants in the presence of different stressors. The indicated *C. glabrata* strains were grown overnight in YPD medium, and cultures were normalized to an OD_{600} of 1.0. Cultures were 10-fold serially diluted in PBS, and $3 \mu\text{l}$ of each dilution was spotted onto YPD medium lacking or containing the indicated compounds. Methyl methanesulfonate (MMS), hydrogen peroxide (H_2O_2), menadione (MD), Congo red (CR), and sodium dodecyl sulfate (SDS) were used at concentrations of 0.03%, 25 mM, $100 \mu\text{M}$, 2 mg/ml, and 0.05%, respectively. All plates were incubated at 30°C unless indicated otherwise. Images were captured after 1 to 2 days of incubation. (B) Time course analysis of the wt, *Cgfp3Δ*, *Cgfp4Δ*, and *Cgfp3Δ4Δ* strains. Cultures grown overnight in YPD medium were reinoculated into fresh YPD medium at an initial OD_{600} of 0.1 and incubated at 30°C . The absorbance of each culture was recorded at regular intervals until 36 h and plotted against time. Data represent means \pm standard errors of the means (SEM) from 5 biological replicates. The growth period between 2 and 8 h, corresponding to the log phase of growth, was used to calculate the doubling time. Data represent means \pm SEM from 5 biological replicates. Unpaired two-tailed Student's *t* test was used to determine the statistical significance of doubling time differences between the wt and the *Cgfp3Δ4Δ* mutant. ****, $P \leq 0.0001$. (C) Representative immunoblots showing histone H3 and H4 levels in the indicated *C. glabrata* strains. Whole-cell extracts of log-phase cultures grown in YPD medium were prepared by the glass bead lysis method. Fifty micrograms of protein was resolved on a 15% SDS-PAGE gel and probed with anti-H3, anti-H4, and anti-GAPDH antibodies. CgGapdh was used as a loading control. For quantification, ImageJ densitometry software was used to measure the intensity of individual bands in 4 independent Western blots. The histone H3 and H4 signals were normalized to the corresponding CgGapdh signal. Data (means \pm SEM; $n=4$) represent percent changes in histone H3 and H4 levels in the *CgfpΔ* mutants compared to the wt strain (considered 100%) and are plotted as a bar graph on the right side of the blot images. *, $P \leq 0.05$; **, $P \leq 0.01$ (by paired two-tailed Student's *t* test). (D) qPCR-based measurement of *CgHHT* (histone H3) and *CgHMF* (histone H4) transcript levels. Using the acid phenol method, total RNA was extracted from log-phase-grown wt and *Cgfp3Δ4Δ* strains. Five hundred nanograms of the total RNA was used to set up real-time quantitative reverse transcriptase PCR. Transcript levels were quantified using the $2^{-\Delta\Delta CT}$ method. Data (means \pm SEM; $n=3$) were normalized against the *CgTDH3* mRNA (which codes for GAPDH) control and represent fold changes in *CgHHT* and *CgHMF* expression in the *Cgfp3Δ4Δ* mutant compared to the wt strain.

and measured their ability to form biofilms on polystyrene-coated plates by a crystal violet stain-based assay. We found that all four strains, wt, *Cgfp3Δ*, *Cgfp4Δ*, and *Cgfp3Δ4Δ*, produced similar amounts of biofilm (Fig. 2A), thereby suggesting that CgFpr3 and CgFpr4 are not required for biofilm formation in *C. glabrata*.

For *in vivo* virulence analysis, we infected BALB/c mice with the wt, *Cgfp3Δ*, *Cgfp4Δ*, and *Cgfp3Δ4Δ* strains through tail vein injections and determined fungal

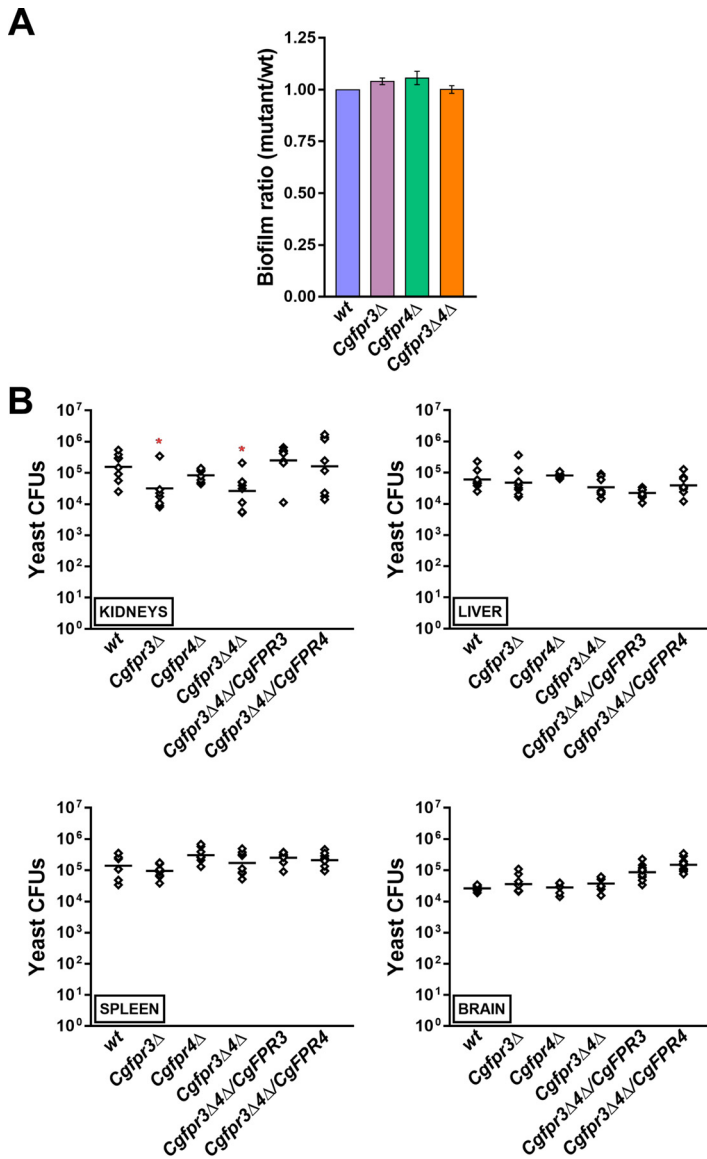


FIG 2 *CgFPR3* and *CgFPR4* are required for virulence. (A) Biofilm formation assay. The wt, *Cgfrp3Δ*, *Cgfrp4Δ*, and *Cgfrp3Δ4Δ* strains were grown in RPMI 1640 medium containing 10% FBS in a 24-well polystyrene plate. After 48 h of incubation, the biofilm formed by yeast cells on polystyrene was stained with 0.4% crystal violet for 45 min, followed by three PBS washes. After destaining with 95% ethanol, the biofilm mass was measured by monitoring the absorbance at 595 nm. Data (means ± SEM; *n* = 3 to 4) represent biofilm ratios, which were calculated by dividing the absorbance units of mutants by those of the wt strain (considered 1.0). (B) Mouse infection assay. BALB/c mice were infected with the indicated *C. glabrata* strains intravenously and sacrificed 7 days after infection. Four organs, kidneys, liver, spleen, and brain, were harvested and homogenized in PBS. The homogenates were appropriately diluted and plated onto YPD medium containing penicillin and streptomycin. The CFU recovered from each organ of the individual mice are plotted. The individual mouse organ CFU are represented by diamonds, while bars mark the CFU geometric means (*n* = 8 to 9) for each organ. *, *P* < 0.05 (by a Mann-Whitney U test).

survival in four target organs, kidneys, liver, spleen, and brain, by a CFU-based assay. We found similar organ fungal burdens in mice infected with the wt and *Cgfrp4Δ* strains (Fig. 2B). In contrast, the *Cgfrp3Δ* and *Cgfrp3Δ4Δ* mutants exhibited about 5-fold fewer CFU in the kidneys of infected mice than in those of wt-infected mice (Fig. 2B). Importantly, the ectopic expression of either *CgFpr3* or *CgFpr4* could rescue the survival defect of the *Cgfrp3Δ4Δ* mutant (Fig. 2B), indicating functional redundancy

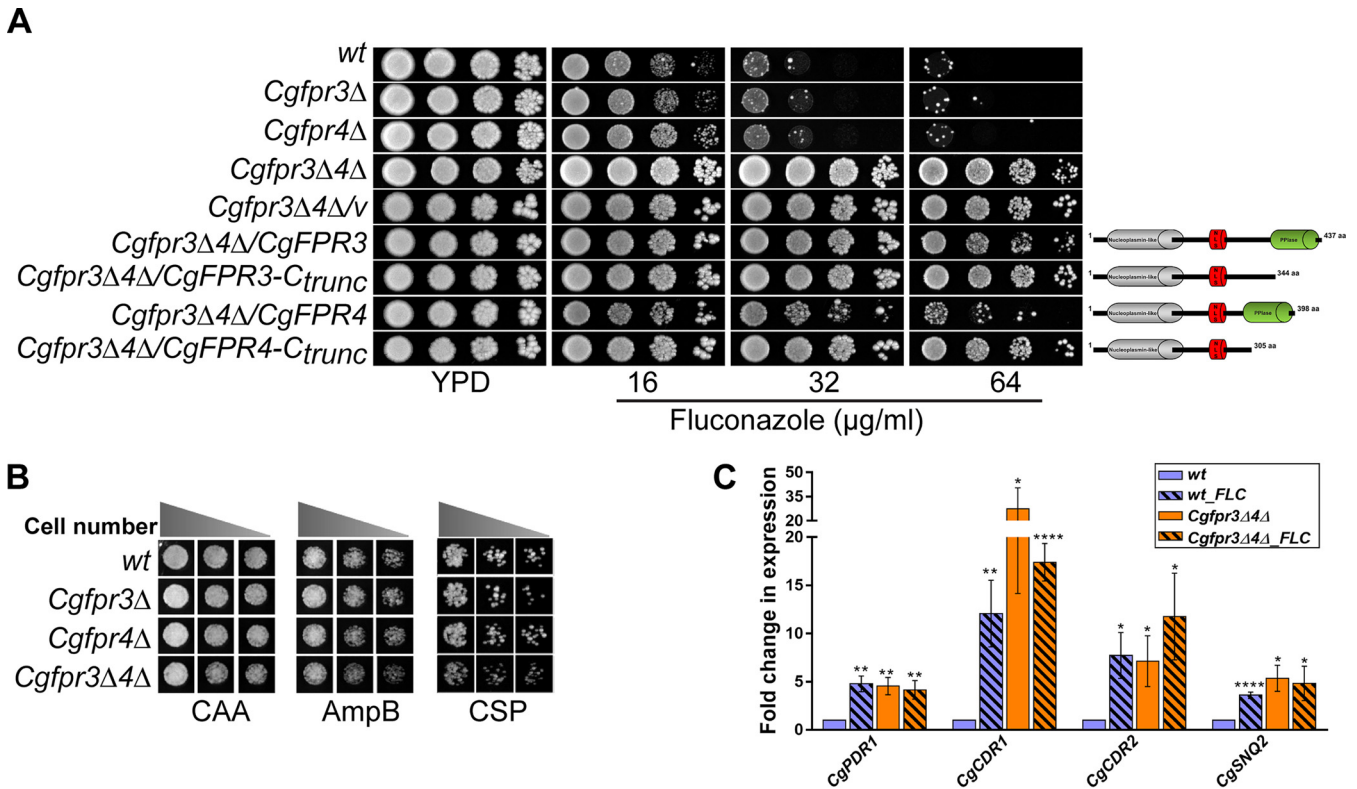


FIG 3 The *Cgfp3*Δ4Δ mutant is resistant to fluconazole. (A) Serial dilution spotting analysis indicating the fluconazole susceptibility of the indicated *C. glabrata* strains. The domain compositions of full-length and C-terminally truncated CgFpr3 and CgFpr4 proteins are shown schematically on the right side of the spotting image. NLS, nuclear localization signal. (B) Liquid medium-based growth analysis of the indicated *C. glabrata* strains to assess sensitivity to amphotericin B and caspofungin. wt and *Cgfp3*Δ mutant strains were grown in Casamino acids medium lacking (CAA) or containing amphotericin B (AmpB) (500 ng/ml) and caspofungin (CSP) (125 ng/ml) at 30°C. After 24 h of incubation, cultures were diluted in PBS, and 3 μl of 100-, 250-, and 500-fold-diluted cultures was spotted onto YPD medium. Images were captured after 1 day of growth at 30°C. (C) qPCR-based quantification of *CgCDR1*, *CgCDR2*, *CgPDR1*, and *CgSNQ2* transcript levels. Log-phase wt and *Cgfp3*Δ4Δ cells were either treated with 16 μg/ml fluconazole for 4 h or left untreated. RNA was extracted, and qPCR was set up using 500 ng of total RNA. Transcript levels were quantified using the $2^{-\Delta\Delta CT}$ method. Data (means ± SEM; $n = 3$ to 5) were normalized against the *CgTDH3* mRNA as a control and represent fold changes in the expression of the *CgCDR1*, *CgCDR2*, *CgPDR1*, and *CgSNQ2* genes in untreated *Cgfp3*Δ4Δ and fluconazole (FLC)-treated wt and *Cgfp3*Δ4Δ cells, compared to the untreated wt cells (taken as 1.0). *, $P \leq 0.0332$; **, $P \leq 0.0021$; ****, $P \leq 0.0001$ (by multiple *t* tests).

between CgFpr3 and CgFpr4 *in vivo* and implicating CgFpr3 and CgFpr4 in the virulence of *C. glabrata* in an organ-dependent manner. In light of these data and the previously reported link between reduced histone H4 gene dosage and diminished virulence (38), it is unlikely that the histone H4 levels *per se* contribute to the fitness of *C. glabrata in vivo*.

***CgFPR3* and *CgFPR4* gene loss led to elevated basal expression of multidrug transporter genes and azole resistance.** As mechanisms governing chromatin architecture and histone lysine acetylation have recently been implicated in resistance to antifungals (28, 29), we next investigated the role of CgFpr3 and CgFpr4 in antifungal drug resistance. For this, we checked the sensitivities of the *Cgfp3*Δ, *Cgfp4*Δ, and *Cgfp3*Δ4Δ mutants to three classes of antifungal drugs, *viz.*, azoles, echinocandins, and polyenes. We found that compared to wt cells, the *Cgfp3*Δ and *Cgfp4*Δ mutants grew slightly better in the presence of the azole antifungal fluconazole (Fig. 3A), while their growth in medium containing the drug amphotericin B (polyene) or caspofungin (echinocandin) was similar to that of the wt strain (Fig. 3B). Intriguingly, the *Cgfp3*Δ4Δ double mutant exhibited a high level of azole resistance, with the mutant exhibiting robust growth in medium containing 64 μg/ml fluconazole (Fig. 3A). Notably, the MIC₈₀s of fluconazole were found to be 16, 16, and 64 μg/ml for the wt, *Cgfp3*Δ, *Cgfp4*Δ, and *Cgfp3*Δ4Δ strains, respectively (Table S1), indicating that the deletion of the *CgFPR3* or *CgFPR4* gene individually had no effect on the fluconazole susceptibility of *C. glabrata*.

Importantly, the ectopic expression of the *CgFPR3* or *CgFPR4* gene reverted the

fluconazole resistance phenotype of the *Cgfp3Δ4Δ* mutant slightly or substantially, respectively (Fig. 3A). The inability of the CgFpr3 and CgFpr4 proteins to fully complement the fluconazole resistance of the *Cgfp3Δ4Δ* mutant could be due to their inadequate expression, functional alterations owing to the C-terminal fusion with green fluorescent protein (GFP), or both proteins being required for each other's full activity. Next, to determine the importance of the PPlase domain of CgFpr3 and CgFpr4 in azole resistance, we generated C-terminally truncated CgFpr3 and CgFpr4 proteins that lacked the PPlase domain and first checked their expression, followed by their ability to complement the azole resistance phenotype of the *Cgfp3Δ4Δ* mutant. Western analysis revealed that both the CgFpr3-C_{trunc} and CgFpr4-C_{trunc} proteins are expressed in the *Cgfp3Δ4Δ* mutant (Fig. S2). However, a reversal of azole resistance in the *Cgfp3Δ4Δ* mutant was not observed upon the expression of CgFpr3 and CgFpr4 proteins that lacked the C-terminal PPlase domain (Fig. 3A), thereby suggesting that the peptidyl-prolyl *cis-trans* isomerase activity of CgFpr3 and CgFpr4, catalyzing the isomerization between the *cis* and *trans* forms of peptide bonds, is pivotal to suppress azole resistance in the *Cgfp3Δ4Δ* mutant. Collectively, these data suggest that CgFpr3 and CgFpr4 negatively regulate the response of *C. glabrata* to azole antifungals and are largely functionally redundant.

Furthermore, FK506 and fluconazole have previously been shown to act synergistically in *C. glabrata* (42). Therefore, we next checked the growth of the wt and the *Cgfp3Δfpr4Δ* mutant in the presence of FK506 and fluconazole. Consistent with the previous report (42), we found a synergistic antifungal effect of fluconazole and FK506 on the growth of wt cells, while the growth of the *Cgfp3Δfpr4Δ* mutant was only mildly retarded (Fig. S3). These results suggest that either the azole resistance in the *Cgfp3Δfpr4Δ* mutant is refractory to the combinatorial inhibitory effect of fluconazole and FK506 or the CgFpr3 and CgFpr4 proteins are required for the synergistic effect of fluconazole and FK506.

Azole exposure in *C. glabrata* leads to the overexpression of the Zn₂Cys₆-type zinc finger motif-containing transcriptional regulator CgPdr1, which in turn activates the expression of the ATP-binding cassette multidrug transporter-encoding genes *CgCDR1*, *CgCDR2*, and *CgSNQ2* (13). As expected, *C. glabrata* wt cells responded to fluconazole exposure by elevating the expression of the *CgPDR1*, *CgCDR1*, *CgCDR2*, and *CgSNQ2* genes by 4- to 12-fold (Fig. 3C). Intriguingly, the *Cgfp3Δ4Δ* mutant exhibited 4.5-fold-higher basal expression levels of the *CgPDR1* gene (Fig. 3C). Consistent with this, basal transcript levels of the *CgCDR1*, *CgCDR2*, and *CgSNQ2* genes, which are target genes of CgPdr1, were 5- to 27-fold higher in the *Cgfp3Δ4Δ* mutant (Fig. 3C). Notably, fluconazole exposure led to no significant increase in *CgPDR1*, *CgCDR1*, *CgCDR2*, and *CgSNQ2* gene expression in the *Cgfp3Δ4Δ* mutant (Fig. 3C), underscoring the lack of fluconazole-induced MDR gene activation in the mutant cells. Altogether, the much higher constitutive levels of the *CgPDR1*, *CgCDR1*, *CgCDR2*, and *CgSNQ2* genes in the *Cgfp3Δ4Δ* mutant suggest that the *CgFPR3* and *CgFPR4* genes negatively regulate CgPdr1-dependent MDR gene expression under regular growth conditions.

Fluconazole exposure led to an increase in histone H3 and H4 protein levels.

The *Cgfp3Δ4Δ* mutant contained elevated histone H3 and H4 protein levels and exhibited higher MDR gene expression levels. Therefore, to further delineate the basis underlying the azole resistance phenotype of the *Cgfp3Δ4Δ* mutant, we checked whether fluconazole exposure modulates histone protein levels in *C. glabrata*. Western analysis revealed that histone H3 and H4 levels were 50 to 60% higher in fluconazole-treated wt cells than in untreated wt cells (Fig. 4A). Contrarily, the *Cgfp3Δ4Δ* mutant did not respond to fluconazole exposure by elevating H3 and H4 levels (Fig. 4A). Of note, histone H4 protein levels are known to be very tightly regulated in *C. glabrata* (38). Importantly, fluconazole treatment had no effect on the transcript levels of the histone H3 and H4 genes in wt cells (Fig. 4B), thereby ruling out fluconazole-responsive transcriptional regulation of H3 and H4 genes. Altogether, these data suggest that *C. glabrata* responds to fluconazole exposure by stabilizing histone H3 and H4 proteins,

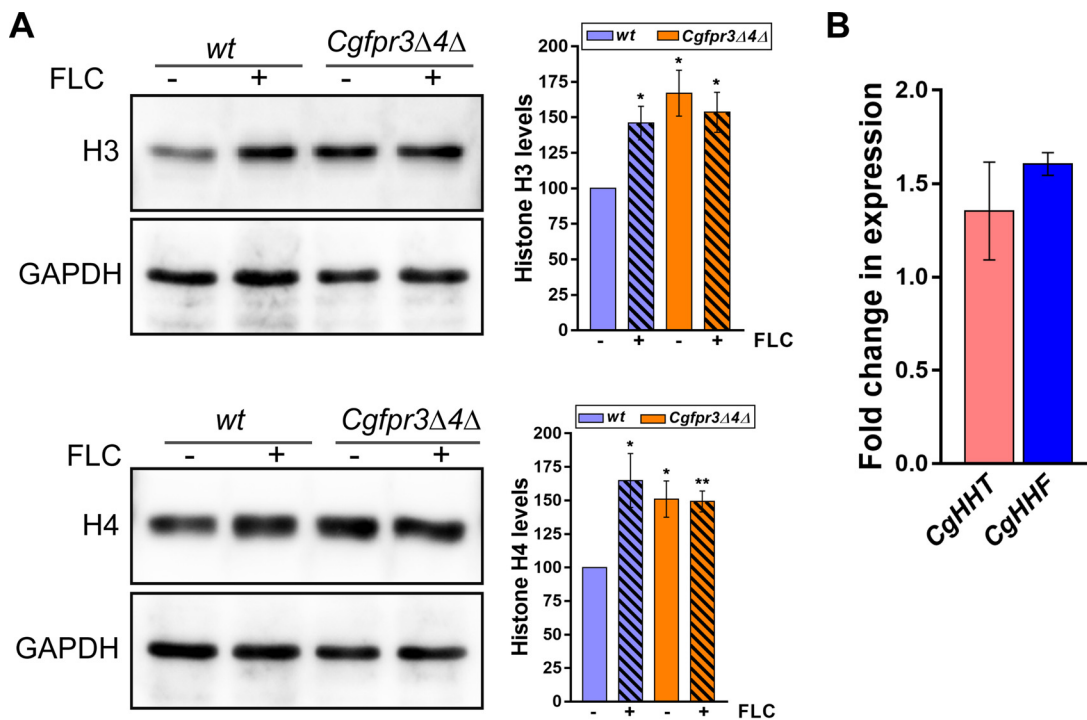


FIG 4 Histone H3 and H4 protein levels are elevated upon fluconazole treatment. (A) Representative immunoblots showing histone H3 and H4 protein levels in fluconazole-treated wt and *Cgfrp3Δ4Δ* cells. Log-phase wt and *Cgfrp3Δ4Δ* cells were either treated with 16 $\mu\text{g/ml}$ fluconazole for 4 h or left untreated. Whole-cell lysates were prepared by glass bead lysis, and 50 μg protein was resolved on 15% SDS-PAGE gels and probed with anti-H3, anti-H4, and anti-GAPDH antibodies. CgGapdh was used as a loading control. The intensity of individual bands from 4 to 5 independent Western blots was quantified using ImageJ densitometry software. H3 and H4 intensity signals were normalized to the corresponding CgGapdh signal. Data (means \pm SEM; $n=4$ to 5) represent the percent changes in histone levels in untreated *Cgfrp3Δ4Δ* and fluconazole (FLC)-treated wt and *Cgfrp3Δ4Δ* cells, compared to the untreated wt cells (considered 100%), and are plotted as a bar graph on the right side of the blot image. *, $P \leq 0.05$; **, $P \leq 0.01$ (by paired two-tailed Student's t test). (B) qPCR-based analysis of *CgHHT* and *CgHHF* gene expression in wt cells upon fluconazole exposure. Log-phase wt cells were either left untreated or treated with 16 $\mu\text{g/ml}$ fluconazole for 4 h. Total RNA (500 ng) was used to set up qPCR, and transcript levels were quantified using the $2^{-\Delta\Delta CT}$ method. Data (means \pm SEM; $n=3$) were normalized against the *CgTDH3* mRNA control and represent fold changes in *CgHHT* and *CgHHF* expression in fluconazole-treated wt cells compared to untreated wt cells (taken as 1.0).

and the inability of the *Cgfrp3Δ4Δ* mutant to augment H3 and H4 upon fluconazole exposure could be due to already elevated H3 and H4 levels in the mutant. In this context, it is noteworthy that cells employ finely tuned regulatory mechanisms to ensure that histone H3 and H4 protein levels are tightly regulated (43).

The mutant lacking the histone demethylase CgRph1 displays diminished expression of MDR genes. Since histone protein stability and functions are modulated by posttranslational modifications (PTMs) (44), we reasoned that CgFpr3 and CgFpr4 may contribute to the maintenance of H3 and H4 levels by regulating their PTMs and that there could be a link between histone PTMs and the azole resistance phenotype of the *Cgfrp3Δ4Δ* mutant. In this context, it is noteworthy that disruption of the *CgSET2* (which encodes a putative histone methyltransferase) and *CgRPH1* (which encodes a putative histone demethylase) genes has recently been reported to result in azole resistance and sensitivity, respectively (45, 46). Importantly, Set2 and Rph1 in *S. cerevisiae* are involved in the methylation and demethylation of histone H3 at lysine residue 36, respectively (47, 48). Furthermore, Fpr4-mediated isomerization of proline residue 38 of histone H3 has been reported to be inhibitory for Set2-mediated methylation of H3 at lysine residue 36 (36). Therefore, to examine the role of histone H3 methylation in azole resistance in *C. glabrata*, we analyzed CgRph1 and CgSet2 protein sequences for the presence of different domains and found that CgRph1 (CAGL0L11880p), a 980-amino-acid (aa) protein, possesses the JmjC domain, involved in histone demethylation reactions, at its N terminus (Fig. S4A). Furthermore, similar to its *S. cerevisiae* ortholog,

the CgSet2 protein contained the SET domain, involved in the methylation of lysine residues, at its N terminus (Fig. S4B).

Next, we generated deletion strains for the *CgSET2* and *CgRPH1* genes, and phenotypic analysis revealed that the *Cgrph1* Δ and *Cgset2* Δ mutants were moderately sensitive and resistant, respectively, to fluconazole (Fig. 5A), in accordance with previous reports (45, 46). The MIC₈₀s of fluconazole were found to be 8 and 32 μ g/ml for the *Cgrph1* Δ and *Cgset2* Δ mutants, respectively (Table S2). We also checked the growth of the *Cgrph1* Δ and *Cgset2* Δ mutants under thermal stress (42°C), DNA damage (methyl methanesulfonate), oxidative stress (hydrogen peroxide and menadione), cell wall stress (Congo red), and cell membrane stress (sodium dodecyl sulfate) conditions and found that the *Cgset2* Δ mutant exhibited elevated susceptibility to SDS stress (Fig. S5). Since Fpr4 restrains the trimethylation of H3K36 in *S. cerevisiae* (36), we next examined the status of the H3K36me3 modification in the *Cgset2* Δ mutant. Western analysis showed that H3K36me3 was largely absent in the *Cgset2* Δ mutant (Fig. 5B), similar to its *S. cerevisiae* counterpart (47), thereby implicating CgSet2 in trimethylation at the H3K36 residue in *C. glabrata*. Of note, appreciable differences in H3K36me3 levels were not observed between the wt and *Cgrph1* Δ strains (Fig. 5B), thereby precluding a role for CgRph1 in controlling global levels of H3K36me3 modification.

Furthermore, to delineate the molecular basis underlying the differential azole susceptibilities of the *Cgrph1* Δ and *Cgset2* Δ mutants, we next quantified the *CgPDR1*, *CgCDR1*, and *CgCDR2* transcript levels in the mutants. Quantitative real-time reverse transcriptase PCR revealed an \sim 2.6- to 3.7-fold downregulation of the *CgPDR1*, *CgCDR1*, and *CgCDR2* genes in the *Cgrph1* Δ mutant (Fig. 5C), which may account for the increased fluconazole susceptibility of the *Cgrph1* Δ mutant. However, despite the fluconazole resistance phenotype of the *Cgset2* Δ mutant, differences in *CgPDR1*, *CgCDR1*, and *CgCDR2* transcript levels between the wt and *Cgset2* Δ strains were not statistically significant (Fig. 5C), suggesting that the global trimethylation at histone H3 lysine residue 36 does not regulate MDR gene expression appreciably in *C. glabrata*. Thus, the molecular basis underlying azole resistance in the *Cgset2* Δ mutant is yet to be elucidated.

The CgPdr1 transcriptional activator is also implicated in the expression regulation of virulence-related genes (12, 18, 22). Since the *Cgrph1* Δ mutant had lower *CgPDR1* gene expression levels, we next examined the virulence potential of the *Cgrph1* Δ and *Cgset2* Δ mutants in the murine model of systemic candidiasis. We found 16- and 3-fold-lower fungal CFU in kidneys and liver, respectively, of *Cgset2* Δ mutant-infected mice than in wt-infected mice (Fig. 5D). In contrast, mice infected with the *Cgrph1* Δ mutant had 140- and 90-fold-lower fungal burdens in liver and spleen, respectively (Fig. 5D). Notably, no significant differences in *C. glabrata* CFU were observed in the brains of mice infected with the wt, *Cgrph1* Δ , or *Cgset2* Δ strain (Fig. 5D). Altogether, these data implicate for the first time the histone demethylase CgRph1 and the histone H3K36 methyltransferase CgSet2 in the survival of *C. glabrata* in mice.

CgCDR1 deletion led to reversal of fluconazole resistance in the *Cgfpr3* Δ 4 Δ mutant. Next, to corroborate that global H3K36 trimethylation levels do not modulate *CgPDR1*-dependent fluconazole resistance, we checked the status of H3K36me3 modification in the wt and azole-resistant *Cgfpr3* Δ 4 Δ mutant strains. Notably, the mutant also had elevated basal expression of the *CgPDR1* and *CgCDR1* genes (Fig. 3C). Western analysis revealed similar basal levels of H3K36me3 in wt and *Cgfpr3* Δ 4 Δ cells (Fig. 6A). Importantly, fluconazole treatment led to no significant change in H3K36me3 levels in either strain (Fig. 6A). Collectively, these data suggest that the cellular response to fluconazole does not involve changes in the global trimethylation of histone H3 at lysine residue 36 in *C. glabrata*.

Finally, to demonstrate that the higher basal levels of expression of the *CgPDR1* and *CgCDR1* genes contribute to azole resistance in the *Cgfpr3* Δ 4 Δ mutant, we generated two triple-deletion strains by deleting either the *CgPDR1* or *CgCDR1* gene in the *Cgfpr3* Δ 4 Δ mutant that lacked the genes encoding two FK506-binding histone chaperone proteins, CgFpr3 and CgFpr4, and checked their sensitivity to fluconazole. As a control, we used

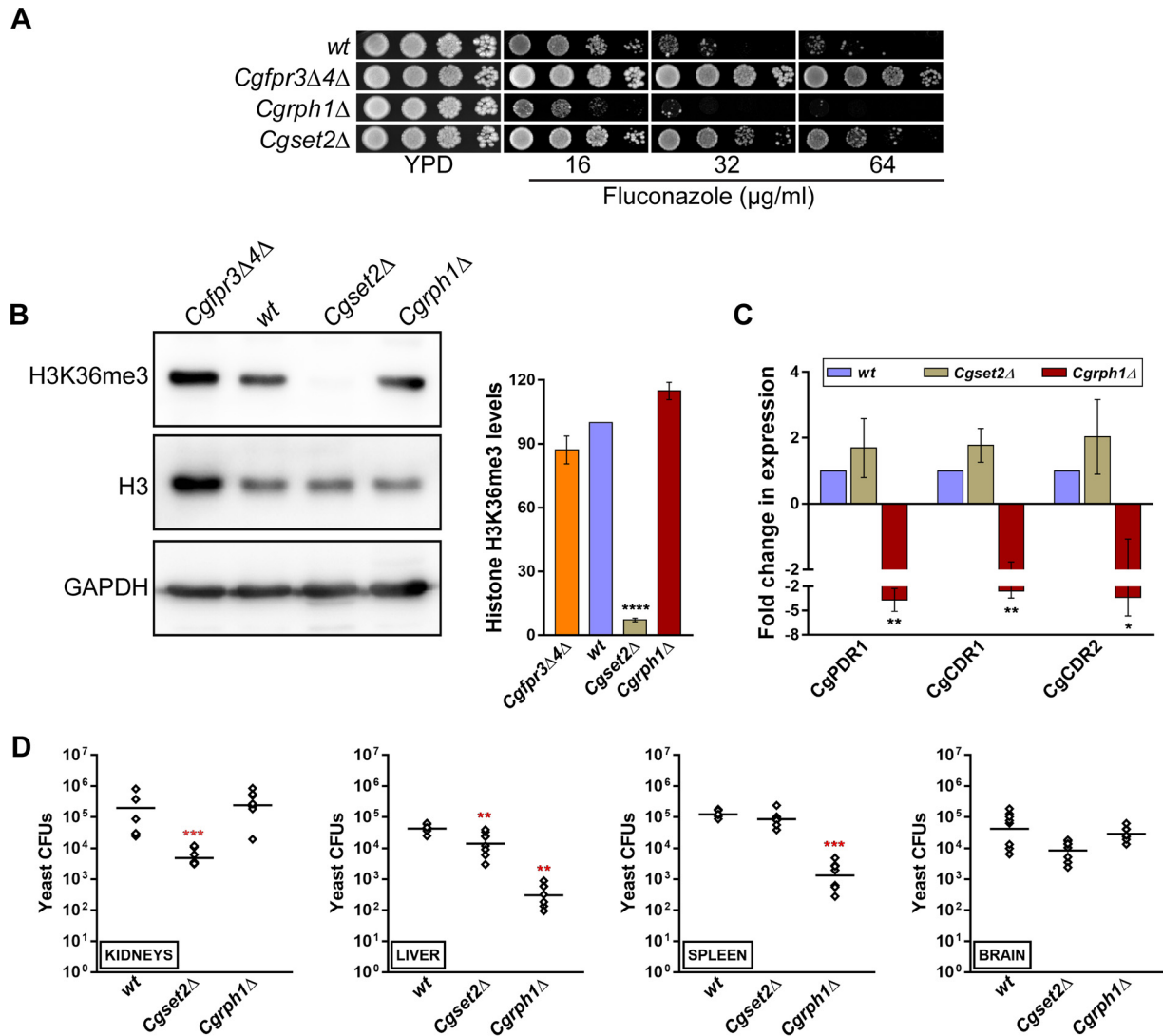


FIG 5 CgSet2 is a histone H3 lysine 36 methyltransferase. (A) Serial dilution spot analysis illustrating the fluconazole susceptibility of the *Cgrph1Δ* and *Cgset2Δ* mutants. Visible artifacts appear within the panels upon overexposure. (B) Representative immunoblots showing H3K36me3 modification levels in the indicated *C. glabrata* strains. Whole-cell lysates of YPD-grown log-phase cultures were prepared, and 50 μ g protein was resolved on a 15% SDS-PAGE gel and probed with anti-H3K36me3, anti-H3, and anti-GAPDH antibodies. GAPDH serves as a loading control. For quantification, the intensity of individual bands from 3 to 4 independent Western blots was measured using ImageJ densitometry software. The histone H3K36me3 signal was normalized to the corresponding total histone H3 signal for each strain. Data (means \pm SEM; $n=3$ to 4) represent the percent changes in histone H3K36me3 levels in mutants compared to the wt strain (considered 100%) and are presented as a bar graph on the right side of the blot image. ****, $P \leq 0.0001$ (by paired two-tailed Student's *t* test). (C) qPCR-based analysis of *CgPDR1*, *CgCDR1*, and *CgCDR2* transcript levels in the wt, *Cgset2Δ*, and *Cgrph1Δ* strains. Data (means \pm SEM; $n=3$ to 4) were normalized against the *CgTDH3* mRNA as a control and represent fold changes in the expression of the *CgPDR1*, *CgCDR1*, and *CgCDR2* genes in the *Cgset2Δ* and *Cgrph1Δ* mutants, compared to the wt strain (considered 1.0). *, $P \leq 0.05$; **, $P \leq 0.01$ (by paired two-tailed Student's *t* test). (D) Organ fungal burden in BALB/c mice infected intravenously with wt, *Cgset2Δ*, or *Cgrph1Δ* *C. glabrata* cells. After 7 days of infection, the fungal burden in the indicated mouse organs was determined by organ collection and homogenization, followed by homogenate plating onto YPD medium containing penicillin and streptomycin. Diamonds and bars represent CFU recovered from organs of the individual mice and the CFU geometric mean ($n=6$ to 8) for each organ, respectively. **, $P \leq 0.01$; ***, $P < 0.001$ (by a Mann-Whitney U test).

Cgpd1Δ and *Cgcd1Δ* mutants, which are supersensitive to fluconazole (Fig. 6B). The *Cgfp3Δ4Δ* mutant showed robust growth in the presence of 64 μ g/ml fluconazole, which was lost upon disruption of the *CgPDR1* or *CgCDR1* gene (Fig. 6B). Interestingly, while the *Cgfp3Δ4Δpd1Δ* triple mutant was unable to grow well even on 4 μ g/ml fluconazole, the *Cgfp3Δ4Δcdr1Δ* mutant exhibited some growth on medium containing 16 μ g/ml fluconazole (Fig. 6B), thereby underscoring the contribution of other multidrug efflux pumps to CgPdr1-mediated azole resistance in the *Cgfp3Δ4Δ* mutant. Importantly, the ectopic

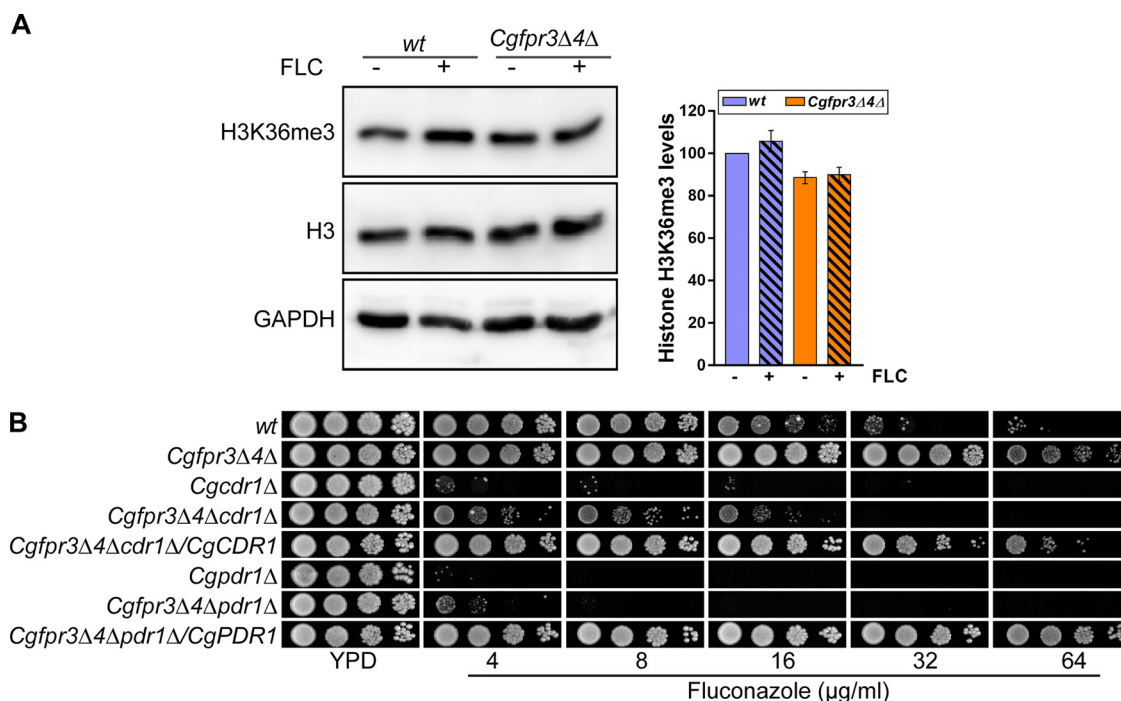


FIG 6 *CgPDR1* or *CgCDR1* disruption reverses azole resistance in the *Cgfp3Δ4Δ* mutant. (A) Representative immunoblots showing H3K36me3 modification levels in the indicated *C. glabrata* strains. Log-phase cultures of wt and *Cgfp3Δ4Δ* cells were either treated with 16 $\mu\text{g/ml}$ fluconazole for 4 h or left untreated. Whole-cell lysates (50 μg protein) were resolved on 15% SDS-PAGE gels and probed with anti-H3K36me3, anti-H3, and anti-GAPDH antibodies. GAPDH serves as a loading control. The intensity signal in each lane was enumerated using ImageJ densitometry software, and the H3K36me3 methylation signal was normalized to the total H3 signal. Data (means \pm SEM; $n=3$ to 4) are plotted as a bar graph on the right side of the blot image and represent the percent changes in H3K36me3 levels in untreated *Cgfp3Δ4Δ* and fluconazole-treated wt and *Cgfp3Δ4Δ* cells, compared to untreated wt samples (considered 100%). (B) Serial dilution spot analysis to assess the fluconazole susceptibility of the indicated *C. glabrata* strains.

expression of *CgPDR1* and *CgCDR1* in the *Cgfp3Δ4Δpdr1Δ* and *Cgfp3Δ4Δcdr1Δ* triple mutants, respectively, restored the fluconazole resistance phenotype of the parental *Cgfp3Δ4Δ* strain (Fig. 6B), indicating that *CgPdr1* and *CgCdr1* overexpression accounts for the azole resistance phenotype of the *Cgfp3Δ4Δ* mutant. Altogether, these data unequivocally link the *CgFpr3* and *CgFpr4* proteins with the regulation of *CgPDR1* and *CgCDR1* gene expression in *C. glabrata*.

In conclusion, we have demonstrated a pivotal role for the first time for FK506-binding histone chaperones in azole resistance via regulation of *CgPdr1*-dependent MDR gene expression (schematically illustrated in Fig. 7) in *C. glabrata*. Additionally, our data point toward epigenetic control of azole antifungal resistance in clinical settings, with the overexpression of multidrug transporters being the most prevalent resistance mechanism.

DISCUSSION

Invasive fungal infections are globally emerging as a significant challenge in hospitals worldwide (49). Treatment of *C. glabrata* infections is particularly difficult due to its intrinsic and acquired antifungal resistance (29, 49). As azole drugs still represent cost-effective, less toxic options for antifungal therapy, there is a compelling need to better understand azole resistance mechanisms and design resistance management strategies. The most clinically prevalent mechanism of azole resistance in *C. glabrata* involves the transcriptional activation of multidrug transporters through gain-of-function mutations in the master regulator-encoding gene *CgPDR1* (12–14). Perturbation of chromatin modifications, including histone acetylation, has been proposed as a promising antifungal therapeutic strategy (28, 29), and HDAC inhibitors are known to act synergistically with azole antifungals (28, 29, 50). Despite this, the precise role of

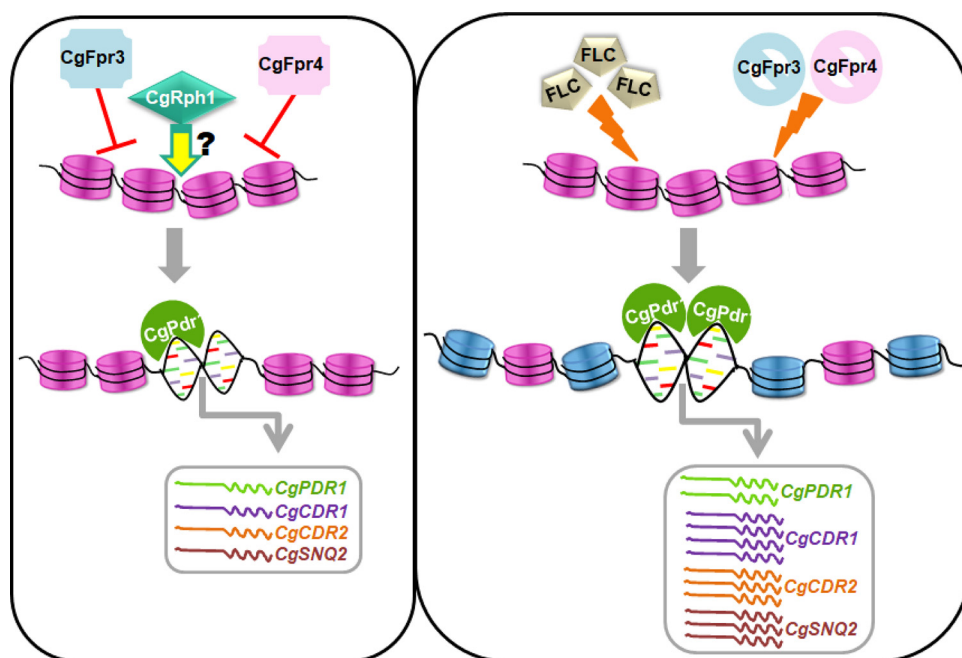


FIG 7 Schematic summarizing the key findings of the study. Under regular growth conditions, the FK506-binding proteins CgFpr3 and CgFpr4 maintain histone H3 and H4 levels and negatively regulate the *CgPDR1* regulon, *viz.*, the expression of the *CgPDR1*, *CgCDR1*, *CgCDR2*, and *CgSNQ2* genes. Contrarily, CgRph1, a putative histone demethylase, positively regulates the *CgPDR1* regulon. Of note, the underlying mechanism(s) is yet to be elucidated. Furthermore, in response to fluconazole exposure or upon the simultaneous deletion of the *CgFPR3* and *CgFPR4* genes, histone H3 and H4 protein levels are elevated, probably leading to differential acetylation and/or methylation of H3 and H4 (represented by blue nucleosomes), and the *CgPDR1* regulon is activated, resulting in the increased expression of the *CgPDR1*, *CgCDR1*, *CgCDR2*, and *CgSNQ2* genes. This activation of MDR genes is pivotal to the survival of fluconazole stress in *C. glabrata*. Of note, the loss of the *CgFPR3* and *CgFPR4* genes leading to an open chromatin state at the *CgPDR1* promoter is yet to be demonstrated experimentally.

histones and histone modification proteins in antifungal resistance in *C. glabrata* remains to be explored (29). Toward this, here, we have elucidated the functions of two putative FK506-binding histone chaperones, CgFpr3 and CgFpr4, in the activation of *CgPDR1* and its target genes *CgCDR1*, *CgCDR2*, and *CgSNQ2*. We show that CgFpr3 and CgFpr4 negatively regulate the expression of the *CgPDR1* regulon and H3 and H4 protein levels. Overall, our work sheds light on the epigenetic networks that modulate the expression of the *CgPDR1* gene, underscoring the multifaceted regulation of ABC transporter gene expression.

CgPdr1, the Cys₆Zn₂ DNA-binding motif-containing transcriptional regulator of pleiotropic drug resistance genes, is a major contributor to azole resistance via the control of both basal and azole-stimulated gene expression (16, 17). CgPdr1 is also known to regulate MDR gene expression by binding directly to azole drugs (51), and CgPdr1 loss results in azole susceptibility (16, 17). CgPdr1 is an autoactivator and regulates the expression of a spectrum of virulence genes, besides MDR genes (18, 22), which highlights its multifunctional roles. Consistent with this, CgPdr1 activity regulation is complex and multifaceted, with diminished *CgERG11* levels and mitochondrial genome loss leading to increased *CgPDR1* expression. Contrarily, the transcription factor CgStb5, the Hsp40 cochaperone CgJjj1, and the deubiquitinase subunit Bre5 act as negative regulators of CgPdr1 levels and/or functions (46, 52, 53). Additionally, the association of CgPdr1 with the CgGal11A subunit of the RNA polymerase II mediator complex also modulates its expression and activity (51, 54). Importantly, the NAD⁺-dependent histone deacetylase CgHst1 has been shown to be a repressor of *CgPDR1* and *CgCDR1* gene expression in *C. glabrata* (31). Our current findings add another regulatory layer

of complexity to this circuitry and point toward histone chaperones also being key players in the CgPdr1-dependent cellular transcriptional response to fluconazole. Although how CgFpr3 and CgFpr4 govern *CgPDR1* expression remains to be determined, one possible mechanism may include azole-stimulated differential recruitment of the regulatory mediator subunit complexes involving CgGal11A/Med15 to *CgPDR1* target gene promoters (54).

An interesting aspect of our work is the increased and decreased susceptibility, arising from the loss of a putative histone demethylase, CgRph1, and H3K36 methyltransferase, CgSet2, respectively, to fluconazole. Although the nexus among CgRph1 and CgSet2 activity, H3K36me3 levels, CgFpr3/4-mediated histone homeostasis, and *CgPDR1* regulon activation is yet to be established, the altered azole susceptibility of the *Cgrph1*Δ and *Cgset2*Δ mutants raises the possibility that cellular metabolism may govern azole stress survival. In this context, it is worth noting that a link between the availability of *S*-adenosylmethionine, which donates a methyl group during reactions catalyzed by methyltransferases, and histone methylation has been well established in higher eukaryotes (55, 56). Intriguingly, transcript levels of the *S*-adenosylmethionine synthetase-encoding gene *SAM2* were found to be elevated in response to itraconazole treatment in *C. albicans* (57). Therefore, it is possible that the histone methylation-dependent regulation of the *CgPDR1* gene is tightly intertwined with the cellular metabolic status that is perturbed upon azole exposure. Future studies will be designed to address this possibility as well as to examine other H3 and H4 methylation modifications in our fluconazole-sensitive (*Cgrph1*Δ) and -resistant (*Cgset2*Δ and *Cgfpr3*Δ4Δ) mutants, as current findings suggest that H3K36me3 is unlikely to be a pivotal determinant of azole resistance.

A multitude of histone modifications have been reported, and growing evidence points to an epigenetic regulation of drug resistance and virulence mechanisms in human-pathogenic fungi, with reversible lysine acetylation and methylation playing pivotal roles (28, 29). The loss of the catalytic subunit (NuB4) of the histone acetyltransferase complex Hat1 has previously been reported to result in elevated azole resistance (58), while the loss of the lysine acetyltransferase Gcn5 (catalytic subunit of the SAGA, SLIK, and ADA histone acetyltransferase complexes) had no effect on azole susceptibility in *C. albicans* (59). Furthermore, HDAC inhibitors are known to act synergistically with azole antifungals in *C. albicans* (50). In accordance, loss of the lysine deacetylases Rpd3 and Hda1 rendered *C. albicans* cells sensitive to azoles (60). However, compared to acetylation, histone methylation is an understudied PTM, and histone methyltransferases and demethylases are yet to be explored for their roles in azole resistance in human fungal pathogens. Of note, our finding that the *Cgrph1*Δ mutant (which lacks a putative histone demethylase) shows increased azole susceptibility raises the possibility of an analogous effect of histone acetylation and methylation on azole resistance. Furthermore, since cross talk between histone methylation and histone acetylation has previously been reported, with H3K36me3 stimulating the acetylation of histone H4 at the K16 residue (61), it is possible that the altered H3K36me3 levels may impact the status of histone acetylation in the *Cgset2*Δ mutant. Of note, histone methylation has also previously been associated with communicating the transcriptional memory of environmental stress responses through mitotic cell divisions in *S. cerevisiae* (62).

Finally, histone chaperones play an important role in chromatin homeostasis via direct binding to histone proteins and regulating the localization, protein levels, interaction, and DNA deposition of histone proteins (63). Histone chaperones belonging to the nucleoplasmin superfamily possess the 8-stranded beta barrel pentameric N-terminal core domain and bind to histones through a predominantly conserved mechanism (64). CgFpr3 and CgFpr4 represent nucleoplasmin-like proteins of this superfamily, and they contain a PPlase domain at their C termini (characteristic of the FKBP class of PPlase enzymes) and are yet to be functionally characterized in *C. glabrata*. *S. cerevisiae* Fpr4 has been shown to localize to the nucleus; bind to the H2B nuclear localization signal sequence; regulate ribosomal DNA (rDNA) silencing, lysine methylation, and

gene expression; and act as an acidic histone chaperone in the assembly of nucleosomal arrays, with its PPlase domain inhibiting the histone chaperone activity (36, 37, 41, 65). Whereas the N-terminal tails of histones H3 and H4 are implicated in binding to Fpr4, the PPlase domain of Fpr4 is involved in the isomerization of proline residues 30 and 38 of H3 (36). Furthermore, *S. cerevisiae* Fpr3 is localized to the nucleolus, forms reversible aggregates upon thermal stress, and assists nucleosome assembly, and its PPlase domain serves as a transcriptional repressor (66–69). *FPR3* and *FPR4* gene deletion in *S. cerevisiae* is also known to result in the differential expression of a wide variety of genes, consistent with their products' roles as histone chaperones (68). Although our data, taken together, suggest that CgFpr3 and CgFpr4 operate largely in a redundant manner and are likely to be functional orthologs of *S. cerevisiae* nuclear FKBP, the mechanism(s) underlying the binding of CgFpr3 and CgFpr4 to histones H3 and H4 and the role of this binding in modulating azole resistance and the cellular status of histone PTMs are yet to be elucidated.

MATERIALS AND METHODS

Strains and media. *C. glabrata* wild-type and mutant strains, which are derivatives of vaginal isolate BG2, were cultured in rich YPD or CAA (Casamino acids) medium at 30°C with shaking at 200 rpm. Bacterial strains were grown at 37°C in LB medium containing 60 µg/ml ampicillin. To obtain logarithmic-phase cells, *C. glabrata* strains were grown overnight in YPD or CAA medium and inoculated into fresh medium at an optical density at 600 nm (OD₆₀₀) of 0.1. After 4 h of growth at 30°C, cultures were pelleted down, and cells were collected. The strains, plasmids, primers, and antibodies used are listed in Tables S3 to S6, respectively, in the supplemental material.

***C. glabrata* gene disruption and cloning.** Using the homologous-recombination-based approach, *C. glabrata* *fpr3Δ*, *fpr4Δ*, *set2Δ*, and *rph1Δ* strains were created with the *nat1* gene (which confers nourseothricin resistance) as a selection marker, as described previously (70). Replacement of the disrupted ORF with the Flp recombination target (FRT)-*nat1* cassette was confirmed by PCR. To create the double-deletion strain, the *Cgfp4Δ* mutant was first transformed with the pRK70 plasmid, which expresses the flip recombinase (enzyme catalyzing recombination at FRT sites)-encoding gene. Transformants were selected for uracil prototrophy and screened for nourseothricin (200 µg/ml) sensitivity after colony purification. Since the *nat1* gene was flipped out of nourseothricin-sensitive *Cgfp4Δ* colonies, these colonies were grown in YPD medium for about 20 generations, followed by the selection of uracil auxotroph colonies. Disruption of the *CgFPR3* gene in the *ura⁻*, nourseothricin-sensitive *Cgfp4Δ* mutant strain was confirmed by PCR. To generate the triple-deletion strain *Cgfp3Δfpr4Δcdr1Δ*, the cassette containing the *nat1* gene flanked with the 5' and 3' untranslated regions (UTRs) of the *CgCDR1* gene was amplified from genomic DNA of the *Cgcdr1Δ* mutant and transformed into the *ura⁻*, nourseothricin-sensitive *Cgfp3Δfpr4Δ* mutant strain. For the generation of C-terminal GFP fusion proteins for mutant complementation studies, *CgFPR3* (*CAGL0L11484g*) (1.31 kb) and *CgFPR4* (*CAGL0M00638g*) (1.19 kb) were cloned into the pRK1018 plasmid between the *PGK1* promoter and the GFP-encoding sequence in the *Xba*I/*Spe*I restriction sites. The clones were verified by PCR and restriction digestion, and the resultant plasmids were transformed into *C. glabrata* strains for complementation analyses.

Quantitative real-time PCR. Log-phase cultures were inoculated at an OD₆₀₀ of 0.1 in YPD medium lacking or containing fluconazole (16 µg/ml) and incubated for 4 h at 30°C in an incubator shaker. Cells were harvested and washed with ice-cold diethyl pyrocarbonate (DEPC)-treated water. Using the acid phenol extraction method, total RNA was extracted and treated with DNase I to remove any residual DNA. cDNA was synthesized by a reverse transcriptase enzyme (SuperScript III first-strand synthesis system for RT-PCR; Invitrogen) using 500 ng of DNase I-digested RNA. Quantitative real-time PCR (qPCR) was performed with the SYBR green qPCR master mix using primers specific for the *CgCDR1*, *CgCDR2*, *CgPDR1*, *CgSNQ2*, *CgHHF*, and *CgHHT* genes and the housekeeping gene *CgTDH3*. *CgTDH3*, which codes for glyceraldehyde-3-phosphate dehydrogenase (GAPDH) and whose expression was not altered upon fluconazole treatment, was used as the reference gene. *C_T* (cycle threshold) values of the *CgCDR1*, *CgCDR2*, *CgPDR1*, *CgSNQ2*, *CgHHF*, and *CgHHT* genes were normalized against the corresponding *C_T* value obtained for the *CgTDH3* gene under similar conditions. The fold change in expression for fluconazole-treated samples compared to untreated samples was calculated by the comparative *C_T* ($2^{-\Delta\Delta C_T}$) method.

Stress susceptibility assays. The susceptibility of *C. glabrata* strains to azole antifungals was evaluated in solid medium by a serial dilution spot assay. For serial dilution spotting analysis, cultures of *C. glabrata* strains grown overnight were normalized to an OD₆₀₀ of 1.0 and serially diluted 10-fold in phosphate-buffered saline (PBS). Three microliters of each dilution was spotted onto YPD medium lacking or containing different concentrations of the azole antifungal fluconazole and other stressors. Plates were incubated at 30°C, and growth was recorded after 24 to 48 h. The liquid growth assay was performed in CAA medium lacking or containing amphotericin B and caspofungin in a 96-well plate. Each well was inoculated with a culture of *C. glabrata* strains grown overnight corresponding to an OD₆₀₀ of 0.2 to a final volume of 100 µl and incubated for 24 h at 30°C. Next, 100-, 250-, and 500-fold culture dilutions were made, and 3 µl of each dilution was spotted onto YPD medium. The plates were incubated at 30°C, and images were captured between 16 and 48 h.

Growth curve analysis. *C. glabrata* wild-type, *Cgfp3Δ*, *Cgfp4Δ*, and *Cgfp3Δ4Δ* mutant strains were grown in 10 ml YPD broth for 16 h at 30°C, followed by inoculation at an OD₆₀₀ of 0.1 in a 100 ml flask

containing 20 ml YPD broth. Cultures were incubated in a shaker incubator at 30°C, and the absorbance was recorded at regular intervals until 36 h.

MIC determination. The MIC was determined using the EUCAST method (71). Briefly, RPMI 1640 medium without sodium bicarbonate was prepared at a 2× concentration and supplemented with 2% glucose and 0.165 M morpholinepropanesulfonic acid (MOPS). The medium pH was adjusted to 7.0 with NaOH and filter sterilized. One hundred microliters of medium lacking or containing various fluconazole concentrations (4, 8, 16, 32, 64, and 128 μg/ml) was added to each well of a 96-well plate. *C. glabrata* wild-type and mutant strains were grown in YPD medium at 30°C at 200 rpm for 16 h and added at a density of 1×10^5 cells/well in the 96-well plate. After incubation at 37°C for 24 h in a moist container, the culture absorbance was recorded visually and measured at 530 nm in the SpectroMax multiplate reader. Endpoints were determined by comparing the OD₅₃₀ values of *C. glabrata* cells grown in the absence and presence of fluconazole. The MIC₈₀ of fluconazole was defined as the lowest drug concentration that inhibited 80% of a strain's growth at 24 h, compared to the control without fluconazole.

Protein extraction and immunoblotting. Log-phase cultures were inoculated at an OD₆₀₀ of 0.1 in YPD medium lacking or containing fluconazole (16 μg/ml) and incubated for 4 h at 30°C in an incubator shaker. Cells were harvested, washed, and suspended in protein extraction buffer (50 mM Tris-HCl [pH 7.5], 2 mM EDTA, 2% glucose) containing 1 mM phenylmethylsulfonyl fluoride, 10 mM sodium fluoride, 1 mM sodium orthovanadate, and a protease inhibitor mixture. Cells were lysed with glass beads using a Fastprep-24 instrument at maximum speed for 60 s five times and spun down at 13,000 rpm for 15 min at 4°C. The proteins were quantified using the bicinchoninic acid (BCA) protein assay kit, run on a 15% SDS-PAGE gel, and immunoblotted with the appropriate antibodies.

Biofilm formation assay. *C. glabrata* cells were grown overnight in YPD medium, suspended in RPMI 1640 medium containing 10% fetal bovine serum (FBS), and seeded at a density of 1×10^7 cells per well in a 24-well polystyrene plate. After a 90 min incubation at 37°C, wells were washed twice with PBS, and fresh RPMI 1640 medium was added. The plate was incubated at 37°C for 48 h, with the removal of spent medium and the addition of RPMI 1640 medium after 24 h. The unbound *C. glabrata* cells were removed, and wells were washed three times with PBS. Crystal violet (0.4% [wt/vol]) stain was added to each well to stain the adherent *C. glabrata* cells. After 45 min, 95% ethanol was added for destaining purposes, followed by absorbance measurement of the destaining solution at 595 nm.

Mouse infection assay. For animal infection, *C. glabrata* strains were grown overnight in YPD medium. After washing with PBS, a 100 μl cell suspension (4×10^7 cells) was injected into the tail vein of 6- to 8-week-old female BALB/c mice. On the 7th day postinfection, mice were sacrificed, and four organs, kidneys, liver, spleen, and brain, were harvested. After homogenizing organs in PBS, appropriate dilutions were plated on YPD medium containing penicillin and streptomycin, and the numbers of *C. glabrata* colonies that appeared after 2 days of incubation at 30°C were counted. Mouse infection procedures were designed to minimize animal suffering, performed at the Animal House Facility of the Centre for DNA Fingerprinting and Diagnostics (CDFD), Hyderabad, India, in accordance with guidelines of the Committee for the Purpose of Control and Supervision of Experiments on Animals, Government of India; and approved by the Institutional Animal Ethics Committee (EAF/RK/CDFD/22).

SUPPLEMENTAL MATERIAL

Supplemental material is available online only.

SUPPLEMENTAL FILE 1, PDF file, 4.2 MB.

ACKNOWLEDGMENTS

This work was supported by a DBT/Wellcome Trust India Alliance senior fellowship to R.K. (IA/S/15/1/501831 [www.indiaalliance.org/]) and grants from the Department of Biotechnology (BT/HRD/NBA/37/01/2014 [www.dbtindia.gov.in/]) and the Science and Engineering Research Board, Department of Science and Technology (EMR/2016/005375 [www.serb.gov.in/]), Government of India. K.K. is a recipient of a Shyama Prasad Mukherjee fellowship of the Council of Scientific and Industrial Research, New Delhi, India (www.csirhrdg.res.in/).

R.M. and K.K. conceived the idea. R.M., K.K., and R.K. designed the study. R.M. and K.K. performed experiments and acquired data. R.M., K.K., and R.K. analyzed data. R.M. and K.K. prepared figures. R.M., K.K., and R.K. wrote the manuscript.

We declare that we have no conflict of interest.

REFERENCES

1. Arendrup MC, Patterson TF. 2017. Multidrug-resistant candida: epidemiology, molecular mechanisms, and treatment. *J Infect Dis* 216:S445–S451. <https://doi.org/10.1093/infdis/jix131>.
2. Kontoyiannis DP. 2017. Antifungal resistance: an emerging reality and a global challenge. *J Infect Dis* 216:S431–S435. <https://doi.org/10.1093/infdis/jix179>.
3. Perlin DS, Rautemaa-Richardson R, Alastruey-Izquierdo A. 2017. The global problem of antifungal resistance: prevalence, mechanisms, and management. *Lancet Infect Dis* 17:e383–e392. [https://doi.org/10.1016/S1473-3099\(17\)30316-X](https://doi.org/10.1016/S1473-3099(17)30316-X).
4. Lewis RE. 2011. Current concepts in antifungal pharmacology. *Mayo Clin Proc* 86:805–817. <https://doi.org/10.4065/mcp.2011.0247>.

5. Anderson TM, Clay MC, Cioffi AG, Diaz KA, Hisao GS, Tuttle MD, Nieuwkoop AJ, Comellas G, Maryum N, Wang S, Uno BE, Wildeman EL, Gonen T, Rienstra CM, Burke MD. 2014. Amphoterin forms an extramembranous and fungicidal sterol sponge. *Nat Chem Biol* 10:400–406. <https://doi.org/10.1038/nchembio.1496>.
6. Pfaller MA, Diekema DJ, Turnidge JD, Castanheira M, Jones RN. 2019. Twenty years of the SENTRY Antifungal Surveillance Program: results for *Candida* species from 1997–2016. *Open Forum Infect Dis* 6:S79–S94. <https://doi.org/10.1093/ofid/ofy358>.
7. Arendrup MC, Dzajic E, Jensen RH, Johansen HK, Kjældgaard P, Knudsen JD, Kristensen L, Leitz C, Lemming LE, Nielsen L, Olesen B, Rosenvinge FS, Røder BL, Schönheyder HC. 2013. Epidemiological changes with potential implication for antifungal prescription recommendations for fungaemia: data from a nationwide fungaemia surveillance programme. *Clin Microbiol Infect* 19:E343–E353. <https://doi.org/10.1111/1469-0691.12212>.
8. Bongomin F, Gago S, Oladele RO, Denning DW. 2017. Global and multi-national prevalence of fungal diseases—estimate precision. *J Fungi* 3:57. <https://doi.org/10.3390/jof3040057>.
9. Chakrabarti A, Sood P, Rudramurthy SM, Chen S, Kaur H, Capoor M, Chhina D, Rao R, Eshwara VK, Xess I, Kindo AJ, Umabala P, Savio J, Patel A, Ray U, Mohan S, Iyer R, Chander J, Arora A, Sardana R, Roy I, Appalaraju B, Sharma A, Shetty A, Khanna N, Marak R, Biswas S, Das S, Harish BN, Joshi S, Mendiratta D. 2015. Incidence, characteristics and outcome of ICU-acquired candidemia in India. *Intensive Care Med* 41:285–295. <https://doi.org/10.1007/s00134-014-3603-2>.
10. Andes DR, Safdar N, Baddley JW, Alexander B, Brumble L, Freifeld A, Hadley S, Herwaldt L, Kauffman C, Lyon GM, Morrison V, Patterson T, Perl T, Walker R, Hess T, Chiller T, Pappas PG, TRANSNET Investigators. 2016. The epidemiology and outcomes of invasive *Candida* infections among organ transplant recipients in the United States: results of the Transplant-Associated Infection Surveillance Network (TRANSNET). *Transpl Infect Dis* 18:921–931. <https://doi.org/10.1111/tid.12613>.
11. Astvad KMT, Johansen HK, Røder BL, Rosenvinge FS, Knudsen JD, Lemming L, Schönheyder HC, Hare RK, Kristensen L, Nielsen L, Gertsen JB, Dzajic E, Pedersen M, Østergård C, Olesen B, Søndergaard TS, Arendrup MC. 2018. Update from a 12-year nationwide fungemia surveillance: increasing intrinsic and acquired resistance causes concern. *J Clin Microbiol* 56:e01564-17. <https://doi.org/10.1128/JCM.01564-17>.
12. Ferrari S, Ischer F, Calabrese D, Posteraro B, Sanguinetti M, Fadda G, Rohde B, Bauser C, Bader O, Sanglard D. 2009. Gain of function mutations in CgPDR1 of *Candida glabrata* not only mediate antifungal resistance but also enhance virulence. *PLoS Pathog* 5:e1000268. <https://doi.org/10.1371/journal.ppat.1000268>.
13. Whaley SG, Rogers PD. 2016. Azole resistance in *Candida glabrata*. *Curr Infect Dis Rep* 18:41. <https://doi.org/10.1007/s11908-016-0554-5>.
14. Cavalheiro M, Costa C, Silva-Dias A, Miranda IM, Wang C, Pais P, Pinto SN, Mil-Homens D, Sato-Okamoto M, Takahashi-Nakaguchi A, Silva RM, Mira NP, Fialho AM, Chibana H, Rodrigues AG, Butler G, Teixeira MC. 2019. A transcriptomics approach to unveiling the mechanisms of *in vitro* evolution towards fluconazole resistance of a *Candida glabrata* clinical isolate. *Antimicrob Agents Chemother* 63:e00995-18. <https://doi.org/10.1128/AAC.00995-18>.
15. Vermitsky JP, Edlind TD. 2004. Azole resistance in *Candida glabrata*: coordinate upregulation of multidrug transporters and evidence for a Pdr1-like transcription factor. *Antimicrob Agents Chemother* 48:3773–3781. <https://doi.org/10.1128/AAC.48.10.3773-3781.2004>.
16. Tsai HF, Krol AA, Sarti KE, Bennett JE. 2006. *Candida glabrata* PDR1, a transcriptional regulator of a pleiotropic drug resistance network, mediates azole resistance in clinical isolates and petite mutants. *Antimicrob Agents Chemother* 50:1384–1392. <https://doi.org/10.1128/AAC.50.4.1384-1392.2006>.
17. Vermitsky JP, Earhart KD, Smith WL, Homayouni R, Edlind TD, Rogers PD. 2006. Pdr1 regulates multidrug resistance in *Candida glabrata*: gene disruption and genome-wide expression studies. *Mol Microbiol* 61:704–722. <https://doi.org/10.1111/j.1365-2958.2006.05235.x>.
18. Caudle KE, Barker KS, Wiederhold NP, Xu L, Homayouni R, Rogers PD. 2011. Genomewide expression profile analysis of the *Candida glabrata* Pdr1 regulon. *Eukaryot Cell* 10:373–383. <https://doi.org/10.1128/EC.00073-10>.
19. Sanglard D, Ischer F, Calabrese D, Majcherzyk PA, Bille J. 1999. The ATP binding cassette transporter gene CgCDR1 from *Candida glabrata* is involved in the resistance of clinical isolates to azole antifungal agents. *Antimicrob Agents Chemother* 43:2753–2765. <https://doi.org/10.1128/AAC.43.11.2753>.
20. Izumikawa K, Kakeya H, Tsai H-F, Grimberg B, Bennett JE. 2003. Function of *Candida glabrata* ABC transporter gene, PDR1. *Yeast* 20:249–261. <https://doi.org/10.1002/yea.962>.
21. Torelli R, Posteraro B, Ferrari S, La Sorda M, Fadda G, Sanglard D, Sanguinetti M. 2008. The ATP-binding cassette transporter-encoding gene CgSNQ2 is contributing to the CgPDR1-dependent azole resistance of *Candida glabrata*. *Mol Microbiol* 68:186–201. <https://doi.org/10.1111/j.1365-2958.2008.06143.x>.
22. Vale-Silva LA, Moeckli B, Torelli R, Posteraro B, Sanguinetti M, Sanglard D. 2016. Upregulation of the adhesin gene *EPA1* mediated by *PDR1* in *Candida glabrata* leads to enhanced host colonization. *mSphere* 1:e00065-15. <https://doi.org/10.1128/mSphere.00065-15>.
23. Vallabhaneni S, Cleveland AA, Farley MM, Harrison LH, Schaffner W, Beldavs ZG, Derado G, Pham CD, Lockhart SR, Smith RM. 2015. Epidemiology and risk factors for echinocandin nonsusceptible *Candida glabrata* bloodstream infections: data from a large multisite population-based candidemia surveillance program, 2008–2014. *Open Forum Infect Dis* 2:ofv163. <https://doi.org/10.1093/ofid/ofv163>.
24. Healey KR, Zhao Y, Perez WB, Lockhart SR, Sobel JD, Farmakiotis D, Kontoyiannis DP, Sanglard D, Taj-Aldeen SJ, Alexander BD, Jimenez-Ortigosa C, Shor E, Perlin DS. 2016. Prevalent mutator genotype identified in fungal pathogen *Candida glabrata* promotes multi-drug resistance. *Nat Commun* 7:11128. <https://doi.org/10.1038/ncomms11128>.
25. Bordallo-Cardona MÁ, Agnelli C, Gómez-Núñez A, Sánchez-Carrillo C, Bouza E, Muñoz P, Escibano P, Guinea J. 2019. MSH2 gene point mutations are not antifungal resistance markers in *Candida glabrata*. *Antimicrob Agents Chemother* 63:e01876-18. <https://doi.org/10.1128/AAC.01876-18>.
26. Singh A, Healey KR, Yadav P, Upadhyaya G, Sachdeva N, Sarma S, Kumar A, Tarai B, Perlin DS, Chowdhary A. 2018. Absence of azole or echinocandin resistance in *Candida glabrata* isolates in India despite background prevalence of strains with defects in the DNA mismatch repair pathway. *Antimicrob Agents Chemother* 62:e00195-18. <https://doi.org/10.1128/AAC.00195-18>.
27. Arastehfar A, Lass-Flörl C, Garcia-Rubio R, Daneshnia F, Ilkit M, Boekhout T, Gabaldon T, Perlin DS. 2020. The quiet and underappreciated rise of drug-resistant invasive fungal pathogens. *J Fungi* 6:138. <https://doi.org/10.3390/jof6030138>.
28. Kuchler K, Jenull S, Shivarathri R, Chauhan N. 2016. Fungal KATs/KDACs: a new highway to better antifungal drugs? *PLoS Pathog* 12:e1005938. <https://doi.org/10.1371/journal.ppat.1005938>.
29. O’Kane CJ, Weild R, Hyland EM. 2020. Chromatin structure and drug resistance in *Candida* spp. *J Fungi* 6:121. <https://doi.org/10.3390/jof6030121>.
30. Schwarzmüller T, Ma B, Hiller E, Istel F, Tscherner M, Brunke S, Ames L, Firon A, Green B, Cabral V, Marcet-Houben M, Jacobsen ID, Quintin J, Seider K, Frohner I, Glaser W, Jungwirth H, Bachelier-Bassi S, Chauvel M, Zeidler U, Ferrandon D, Gabaldón T, Hube B, d’Enfert C, Rupp S, Cormack B, Haynes K, Kuchler K. 2014. Systematic phenotyping of a large-scale *Candida glabrata* deletion collection reveals novel antifungal tolerance genes. *PLoS Pathog* 10:e1004211. <https://doi.org/10.1371/journal.ppat.1004211>.
31. Orta-Zavalza E, Guerrero-Serrano G, Gutiérrez-Escobedo G, Cañas-Villamar I, Juárez-Cepeda J, Castaño I, De Las Peñas A. 2013. Local silencing controls the oxidative stress response and the multidrug resistance in *Candida glabrata*. *Mol Microbiol* 88:1135–1148. <https://doi.org/10.1111/mmi.12247>.
32. Pfaller MA, Messer SA, Georgopapadakou N, Martell LA, Besterman JM, Diekema DJ. 2009. Activity of MGCD290, a Hos2 histone deacetylase inhibitor, in combination with azole antifungals against opportunistic fungal pathogens. *J Clin Microbiol* 47:3797–3804. <https://doi.org/10.1128/JCM.00618-09>.
33. Rai MN, Balusu S, Gorityala N, Dandu L, Kaur R. 2012. Functional genomic analysis of *Candida glabrata*-macrophage interaction: role of chromatin remodeling in virulence. *PLoS Pathog* 8:e1002863. <https://doi.org/10.1371/journal.ppat.1002863>.
34. Dolinski K, Muir S, Cardenas M, Heitman J. 1997. All cyclophilins and FK506 binding proteins are, individually and collectively, dispensable for viability in *Saccharomyces cerevisiae*. *Proc Natl Acad Sci U S A* 94:13093–13098. <https://doi.org/10.1073/pnas.94.24.13093>.
35. Davey M, Hannam C, Wong C, Brandl CJ. 2000. The yeast peptidyl proline isomerases FPR3 and FPR4, in high copy numbers, suppress defects resulting from the absence of the E3 ubiquitin ligase TOM1. *Mol Genet* 263:520–526. <https://doi.org/10.1007/s004380051197>.
36. Nelson CJ, Santos-Rosa H, Kouzarides T. 2006. Proline isomerization of histone H3 regulates lysine methylation and gene expression. *Cell* 126:905–916. <https://doi.org/10.1016/j.cell.2006.07.026>.

37. Xiao H, Jackson V, Lei M. 2006. The FK506-binding protein, Fpr4, is an acidic histone chaperone. *FEBS Lett* 580:4357–4364. <https://doi.org/10.1016/j.febslet.2006.06.093>.
38. Kumar K, Moirangthem R, Kaur R. 2020. Histone H4 dosage modulates DNA damage response in the pathogenic yeast *Candida glabrata* via homologous recombination pathway. *PLoS Genet* 16:e1008620. <https://doi.org/10.1371/journal.pgen.1008620>.
39. Eirín-López JM, Frehlick LJ, Ausió J. 2006. Long-term evolution and functional diversification in the members of the nucleophosmin/nucleoplamin family of nuclear chaperones. *Genetics* 173:1835–1850. <https://doi.org/10.1534/genetics.106.058990>.
40. Ohkuni K, Abdulle R, Kitagawa K. 2014. Degradation of centromeric histone H3 variant Cse4 requires the Fpr3 peptidyl-prolyl cis-trans isomerase. *Genetics* 196:1041–1045. <https://doi.org/10.1534/genetics.114.161224>.
41. Shan X, Xue Z, Mélése T. 1994. Yeast NPI46 encodes a novel prolyl cis-trans isomerase that is located in the nucleolus. *J Cell Biol* 126:853–862. <https://doi.org/10.1083/jcb.126.4.853>.
42. Kaur R, Castano I, Cormack BP. 2004. Functional genomic analysis of fluconazole susceptibility in the pathogenic yeast *Candida glabrata*: roles of calcium signaling and mitochondria. *Antimicrob Agents Chemother* 48:1600–1613. <https://doi.org/10.1128/aac.48.5.1600-1613.2004>.
43. Gunjan A, Paik J, Verreault A. 2006. The emergence of regulated histone proteolysis. *Curr Opin Genet Dev* 16:112–118. <https://doi.org/10.1016/j.gde.2006.02.010>.
44. O’Kane CJ, Hyland EM. 2019. Yeast epigenetics: the inheritance of histone modification states. *Biosci Rep* 39:BSR20182006. <https://doi.org/10.1042/BSR20182006>.
45. Bhakt P, Shivarathri R, Choudhary DK, Borah S, Kaur R. 2018. Fluconazole-induced actin cytoskeleton remodeling requires phosphatidylinositol 3-phosphate 5-kinase in the pathogenic yeast *Candida glabrata*. *Mol Microbiol* 110:425–443. <https://doi.org/10.1111/mmi.14110>.
46. Whaley SG, Caudle KE, Simonicova L, Zhang Q, Moye-Rowley WS, Rogers PD. 2018. Jjj1 is a negative regulator of Pdr1-mediated fluconazole resistance in *Candida glabrata*. *mSphere* 3:e00466-17. <https://doi.org/10.1128/mSphere.00466-17>.
47. Strahl BD, Grant PA, Briggs SD, Sun Z-W, Bone JR, Caldwell JA, Mollah S, Cook RG, Shabanowitz J, Hunt DF, Allis CD. 2002. Set2 is a nucleosomal histone H3-selective methyltransferase that mediates transcriptional repression. *Mol Cell Biol* 22:1298–1306. <https://doi.org/10.1128/mcb.22.5.1298-1306.2002>.
48. Klose RJ, Gardner KE, Liang G, Erdjument-Bromage H, Tempst P, Zhang Y. 2007. Demethylation of histone H3K36 and H3K9 by Rph1: a vestige of an H3K9 methylation system in *Saccharomyces cerevisiae*? *Mol Cell Biol* 27:3951–3961. <https://doi.org/10.1128/MCB.02180-06>.
49. Denning DW, Bromley MJ. 2015. How to bolster the antifungal pipeline. *Science* 347:1414–1416. <https://doi.org/10.1126/science.aaa6097>.
50. Smith WL, Edlind TD. 2002. Histone deacetylase inhibitors enhance *Candida albicans* sensitivity to azoles and related antifungals: correlation with reduction in CDR and ERG upregulation. *Antimicrob Agents Chemother* 46:3532–3539. <https://doi.org/10.1128/aac.46.11.3532-3539.2002>.
51. Thakur JK, Arthanari H, Yang F, Pan SJ, Fan X, Breger J, Frueh DP, Gulshan K, Li DK, Mylonakis E, Struhl K, Moye-Rowley WS, Cormack BP, Wagner G, Näär AM. 2008. A nuclear receptor-like pathway regulating multidrug resistance in fungi. *Nature* 452:604–609. <https://doi.org/10.1038/nature06836>.
52. Noble JA, Tsai HF, Suffis SD, Su Q, Myers TG, Bennett JE. 2013. STB5 is a negative regulator of azole resistance in *Candida glabrata*. *Antimicrob Agents Chemother* 57:959–967. <https://doi.org/10.1128/AAC.01278-12>.
53. Paul S, McDonald WH, Moye-Rowley WS. 2018. Negative regulation of *Candida glabrata* Pdr1 by the deubiquitinase subunit Bre5 occurs in a ubiquitin independent manner. *Mol Microbiol* 110:309–323. <https://doi.org/10.1111/mmi.14109>.
54. Nishikawa JL, Boeszoermenyi A, Vale-Silva LA, Torelli R, Posteraro B, Sohn YJ, Ji F, Gelev V, Sanglard D, Sanguinetti M, Sadreyev RI, Mukherjee G, Bhyravabhotla J, Buhrlage SJ, Gray NS, Wagner G, Naar AM, Arthanari H. 2016. Inhibiting fungal multidrug resistance by disrupting an activator-mediator interaction. *Nature* 530:485–489. <https://doi.org/10.1038/nature16963>.
55. Mentch SJ, Mehrmohamadi M, Huang L, Liu X, Gupta D, Mattocks D, Gómez Padilla P, Ables G, Bamman MM, Thalacker-Mercer AE, Nichenametla SN, Locasale JW. 2015. Histone methylation dynamics and gene regulation occur through the sensing of one-carbon metabolism. *Cell Metab* 22:861–873. <https://doi.org/10.1016/j.cmet.2015.08.024>.
56. Serefidou M, Venkatasubramani AV, Imhof A. 2019. The impact of one carbon metabolism on histone methylation. *Front Genet* 10:764. <https://doi.org/10.3389/fgene.2019.00764>.
57. De Backer MD, Ilyina T, Ma XJ, Vandoninck S, Luyten WHML, Vanden Bossche H. 2001. Genomic profiling of the response of *Candida albicans* to itraconazole treatment using a DNA microarray. *Antimicrob Agents Chemother* 45:1660–1670. <https://doi.org/10.1128/AAC.45.6.1660-1670.2001>.
58. Tscherner M, Zwolanek F, Jenull S, Sedlazeck FJ, Petryshyn A, Frohner IE, Mavrianos J, Chauhan N, von Haeseler A, Kuchler K. 2015. The *Candida albicans* histone acetyltransferase Hat1 regulates stress resistance and virulence via distinct chromatin assembly pathways. *PLoS Pathog* 11:e1005218. <https://doi.org/10.1371/journal.ppat.1005218>.
59. Shivarathri R, Tscherner M, Zwolanek F, Singh NK, Chauhan N, Kuchler K. 2019. The fungal histone acetyl transferase Gcn5 controls virulence of the human pathogen *Candida albicans* through multiple pathways. *Sci Rep* 9:9445. <https://doi.org/10.1038/s41598-019-45817-5>.
60. Li X, Cai Q, Mei H, Zhou X, Shen Y, Li D, Liu W. 2015. The Rpd3/Hda1 family of histone deacetylases regulates azole resistance in *Candida albicans*. *J Antimicrob Chemother* 70:1993–2003. <https://doi.org/10.1093/jac/dkv070>.
61. Li L, Wang Y. 2017. Cross-talk between the H3K36me3 and H4K16ac histone epigenetic marks in DNA double-strand break repair. *J Biol Chem* 292:11951–11959. <https://doi.org/10.1074/jbc.M117.788224>.
62. Fabrizio P, Garvis S, Palladino F. 2019. Histone methylation and memory of environmental stress. *Cells* 8:339. <https://doi.org/10.3390/cells8040339>.
63. Burgess RJ, Zhang Z. 2013. Histone chaperones in nucleosome assembly and human disease. *Nat Struct Mol Biol* 20:14–22. <https://doi.org/10.1038/nsmb.2461>.
64. Namboodiri VMH, Akey IV, Schmidt-Zachmann MS, Head JF, Akey CW. 2004. The structure and function of Xenopus NO38-core, a histone chaperone in the nucleolus. *Structure* 12:2149–2160. <https://doi.org/10.1016/j.str.2004.09.017>.
65. Kuzuhara T, Horikoshi M. 2004. A nuclear FK506-binding protein is a histone chaperone regulating rDNA silencing. *Nat Struct Mol Biol* 11:275–283. <https://doi.org/10.1038/nsmb733>.
66. Manning-Krieg UC, Henriquez R, Cammas F, Graff P, Gavériaux S, Movva NR. 1994. Purification of FKBP-70, a novel immunophilin from *Saccharomyces cerevisiae*, and cloning of its structural gene, FPR3. *FEBS Lett* 352:98–103. [https://doi.org/10.1016/0014-5793\(94\)00927-9](https://doi.org/10.1016/0014-5793(94)00927-9).
67. Benton BM, Zang JH, Thorner J. 1994. A novel FK506- and rapamycin-binding protein (FPR3 gene product) in the yeast *Saccharomyces cerevisiae* is a proline rotamase localized to the nucleolus. *J Cell Biol* 127:623–639. <https://doi.org/10.1083/jcb.127.3.623>.
68. Park SK, Xiao H, Lei M. 2014. Nuclear FKBP, Fpr3 and Fpr4 affect genome-wide genes transcription. *Mol Genet Genomics* 289:125–136. <https://doi.org/10.1007/s00438-013-0794-0>.
69. Wallace EWJ, Kear-Scott JL, Pilipenko EV, Schwartz MH, Laskowski PR, Rojek AE, Katanski CD, Riback JA, Dion MF, Franks AM, Airoidi EM, Pan T, Budnik BA, Drummond DA. 2015. Reversible, specific, active aggregates of endogenous proteins assemble upon heat stress. *Cell* 162:1286–1298. <https://doi.org/10.1016/j.cell.2015.08.041>.
70. Borah S, Shivarathri R, Kaur R. 2011. The Rho1 GTPase-activating protein CgBem2 is required for survival of azole stress in *Candida glabrata*. *J Biol Chem* 286:34311–34324. <https://doi.org/10.1074/jbc.M111.264671>.
71. Rodriguez-Tudela JL, Arendrup MC, Barchiesi F, Bille J, Chryssanthou E, Cuenca-Estrella M, Dannaoui E, Denning DW, Donnelly JP, Dromer F, Fegeler W, Lass-Flörl C, Moore C, Richardson M, Sandven P, Velegriaki A, Verweij P. 2008. EUCAST definitive document EDef 7.1: method for the determination of broth dilution MICs of antifungal agents for fermentative yeasts. *Clin Microbiol Infect* 14:398–405. <https://doi.org/10.1111/j.1469-0691.2007.01935.x>.